STATISTICS, OPTIMIZATION AND INFORMATION COMPUTING
Stat., Optim. Inf. Comput., Vol. **14**, December 2025, pp 3667–3705.
Published online in International Academic Press (www.IAPress.org)

Modeling the Impacts of Vaccination and other Interventions on Malaria Transmission Dynamics

Ayodeji Sunday Afolabi [1,2], Miswanto Miswanto [2,*]

[1]*Department of Mathematical Sciences, Federal University of Technology, Akure, P.M.B. 704, Akure, Ondo State, Nigeria*
[2]*Department of Mathematics, Faculty of Sciences and Technology, Airlangga University, Surabaya, Indonesia*

Abstract Malaria remains a persistent global health challenge, with its burden concentrated in Sub-Saharan Africa and other endemic regions where transmission is sustained by interactions between human and mosquito populations. Despite progress in prevention and treatment, the emergence of partial immunity, asymptomatic carriers, and insecticide resistance complicates control efforts. In this study, we formulate and analyze a nonlinear compartmental model that incorporates a vaccination class alongside traditional malaria interventions. The model's mathematical properties are established by proving the positivity and boundedness of solutions, and by deriving the disease-free and endemic equilibria. Using the Diekmann-Heesterbeek-Metz Next Generation Matrix approach, we obtain the effective reproduction number and conduct rigorous local and global stability analyses of both equilibria. Furthermore, local sensitivity analysis is performed to identify key parameters driving transmission, highlighting the roles of vaccine uptake, waning immunity, mosquito–human contact rate, and vaccine efficacy. Numerical simulations illustrate the epidemiological impact of vaccination, showing that increased vaccine coverage substantially reduces infection prevalence and sustains lower transmission levels. To complement this, we extend the analysis with a cost-effectiveness evaluation of three optimal control strategies combining insecticide-treated nets, diagnostic surveillance, and environmental sanitation. The results show that while single or dual interventions moderately reduce infections, the integrated triple-intervention strategy together with the vaccinated compartment achieves the greatest epidemiological impact while also being the most cost-effective, yielding the lowest ACER and a negative ICER, indicating cost savings. These findings emphasize that vaccination, when combined with other interventions, not only reduces malaria burden but also represents an economically justified approach to sustainable control.

Keywords malaria, Anopheles mosquitoes, vaccination, nonlinear dynamics, stability analysis, sensitivity analysis, optimal control, cost-effectiveness

DOI: 10.19139/soic-2310-5070-2582

1. Introduction

Malaria is a disease that is caused by protozoan parasites, a member of Plasmodium genus family and it is highly infectious. Plasmodium falciparum is the most virulent member of this family and it accounts for the majority of malaria-related motalities worldwide. Susceptible individuals contract malaria when they are bitten by female Anopheles mosquitoes carrying the infection, leading to severe illnesses in some individuals. The first sign of malaria infection usually occur between $10-15$ days after coming in contact with the the parasite. However, other forms of transmission occasionally occur, including through blood transfusion, needle sharing, nosocomial infection, organ transplantation, or vertical transmission from mother to fetus [56, 57, 58]

Malaria is widespread in various regions, including large areas of Africa, Latin America, parts of the Caribbean, Eastern Europe, the South Pacific, and significant portions of Asia, such as South Asia, Southeast Asia, and the

*Correspondence to: Miswanto Miswanto (Email: miswanto@fst.unair.ac.id). Department of Mathematics, Faculty of Sciences and Technology, Airlangga University, Surabaya, Indonesia

ISSN 2310-5070 (online) ISSN 2311-004X (print)

Middle East. These regions have favorable conditions for mosquito breeding and are considered endemic to the disease due to the continuous presence of the disease. About 50% of the population of the world are vulnerable to malaria transmission. In regions where malaria is endemic, some individuals develop partial immunity over time due to repeated exposure to the parasite. It should be noted that this partial immunity does not offer complete protection, it however significantly lowers the likelihood of severity of the disease and chances of death from the infections. Many of the individuals who have acquired partial immunity exhibit no visible symptoms despite carrying the parasite. This can complicate detection and control efforts, as asymptomatic individuals can still contribute to the transmission of malaria. Most malaria-related deaths occur in young children in high-transmission areas, such as West Africa because their immune system are not fully developed. In these areas, children under five are particularly vulnerable to severe malaria and malaria-related deaths. Consequently, the need for an effective strategy aimed at reaching the most vulnerable populations has been introduced [58, 59]

Malaria remains a persistent epidemiological issue, especially in tropical and subtropical zones, where its transmission dynamics are strongly influenced by factors such as ecological and climatic changes. In view of this, scientists from different fields including mathematicians have come up with different strategies to curtail malaria in different regions of the world. A number of mathematical models that can help to check the prevalence of malaria have been developed over the years [1, 2, 8, 13, 17, 20, 21, 23, 24, 34, 36, 38, 39, 41, 42, 43, 44, 45, 61, 63, 64, 68, 72, 82, 83, 84]. [40] studied the history and effects of mathematical models for the transmission dynamics and control of malaria for over a century. This study became necessary due to the fact that malaria continue to thrive and post a significant threat to human health, contributing to rising mortality and morbidity rates, driven by environmental changes and socio-economic factors that influence vector ecology, transmission dynamics, and healthcare accessibility. Hence, existing malaria models were critically examined in order to determine their effectiveness in representing host-parasite dynamics. A hierarchical framework of deterministic mathematical models with varying levels of complexity was generated and the modeling strategies adopted were examined. Findings from these reviews may guide researchers in developing more appropriate models that capture current realities such as resistance, vaccination etc. [52] proposed a seven-dimensional ordinary differential equation (ODE) model that described the transmission dynamics of Plasmodium falciparum malaria between humans and mosquito subpopulations with non-linear infection forces denoted by saturated incidence rates. The research identified the region where the model remains epidemiologically viable. Numerical simulations were conducted in order to determine the behaviors of the model classes under certain conditions. [5] developed a mathematical model for malaria and vector subpopulations incorperating traditional malaria intervention measures implemented by proactive individuals. The study demonstrated that the importation of malaria cases had a potential of altering the reproductive number, $(\mathcal{R}_0)$, thereby influencing local epidemiological patterns. Consequently, the findings suggested that full vigilance in implementing both WHO-endorsed and traditional malaria intervention measures represented the most effective strategy for fighting the influence of malaria importation.

A malaria model incorporating temperature dependence and the developmental stages of mosquitoes was developed and analyzed. The model parameters were expressed as periodic functions. The vector and effective reproduction numbers associated with the model were obtained. Whenever the two reproduction numbers surpass one, the system exhibited a minimum of one positive periodic solution and the disease persisted. Numerical simulations were carried out using monthly mean temperature values from Burkina Faso and the results agreed favourably well with the theoretical findings [71] .

[33] modeled the growth rate of awareness programs targeting the population as being proportional to the number of unaware infected individuals. It was assumed that, based on these awareness campaigns, individuals who were infected with the disease became aware of their condition thereby adopting behavioral modifications that limit their exposure to mosquitoes. The model was simulated using Runge$-$Kutta method and the results indicated a substantial increase in the population of susceptible individuals and a decrease in the number of infected mosquitoes. [73] assumed that there was no vertical transmission and that all the newborns were vulnerable to malaria infection. The results revealed that the population of susceptible individuals would continue to increase because of new births and immune waning of the recovered population. Thus, the authors asserted that malaria would continue to be increasingly endemic.

[7] formulated a mathematical model consisting of some control strategies that would significantly reduce the number of infected individuals and mosquito population. The numerical simulation revealed the optimal level needed to minimize the incidence rate. [51] proposed and explored the transmission dynamics of malaria within a population using a non-linear mathematical model. The stability theory of differential equations was used to analyze the model. The model was extended to an OCP by incorporating three time-dependent control measures - bed nets, treatment and insecticides. Optimal control theory was employed to characterize the control variables. Fourth-order forward-backward Runge-Kutta method was adopted for the solution of the extended model. The impacts of these control strategies on the prevalence of malaria-infected individuals were analyzed. Different combination of the control strategies investigated.

1.1. Malaria Vaccines and its Effects

In 2021, World Health Organization (WHO) endorsed RTS,S/AS01 (RTS,S) vaccine for malaria prevention in children living in regions with moderate to high Plasmodium falciparum transmission. At least one dose of this vaccine was administered to over 2 million children in Ghana, Kenya, and Malawi under the supervision of WHO. A comprehensive evaluation revealed a significant reduction in severe malaria cases and a 13% reduction in early childhood mortality in regions where the RTS,S vaccine was administered compared to areas without its introduction [55]. [62] studied the implementation of RTS,S/AS01 malaria vaccine in sub-Saharan Africa (SSA). It was noted that 30 out of the 34 countries in SSA have requested GAVI for financial support and access to the vaccine and 20 out of the 30 countries have been approved. However, the implementation of the vaccine has been limited to only the three pilot countries designated by the WHO - Kenya, Ghana and Malawi and only two non-pilot countries Burkina Faso and Cameroon. In view of this, [26] proposed a mathematical model that captured the administration of this vaccine for children in Kenya, Ghana, and Malawi. In addition to the incorporation of vaccinated class into the model, the inflow of infected immigrants was also considered. The model analysis indicated that when there were no infected immigrant, the disease-free equilibrium point (DFE) was globally symptomatically stable (GAS) when $\mathcal{R}_0 < 1$. However, the model exhibited only endemic equilibrium states with the influx of infected immigrants. Sensitivity analysis of $\mathcal{R}_0$ indicated the importance of reducing human-vector contact. The results showed that increasing children's vaccination rate and elimination of infected human inflows could help to achieve a malaria-free population. The analysis and simulation of the optimal control problem (OCP) demonstrated that the most effective measure of eliminating malaria is the combined use of vaccination, personal protective measures, and treatment contingent upon the complete cessation of infected immigrant inflows. [69] formulated a two-group malaria model structured by age, incorporating vaccination for children under 5 years. The existence of multiple endemic equilibria was explored using Descartes' rule of signs. A global sensitivity analysis (GSA) of $\mathcal{R}_0$ together with the response functions of the vaccination compartment was conducted using partial rank correlation coefficients embedded in Latin Hypercube Sampling. Optimal control theory was employed to obtain the best combination of control strategies for minimizing malaria transmission. In a community, the simultaneous implementation of the three intervention measures could significantly enhance malaria control efforts. The importance of such strategies has been reinforced by recent developments in malaria prevention. In October 2023, WHO recommended R21/Matrix-M malaria vaccine as a second safe and effective option for malaria prevention. The availability of 2 malaria vaccines is expected to increase supply and make broad-scale deployment across Africa and beyond possible [62, 57].

2. Model Formulation and Analysis

A malaria model represented by the system of ten ODEs that captures the dynamics of malaria transmission between human and mosquito populations is proposed. The human population is divided into Susceptible (S_h), Vaccinated (V_h), Exposed (E_h), Asymptomatic Infected (A_h), Infected (I_h), Treated (T_h), Recovered (R_h) while the mosquitoes population is partitioned into Susceptible (S_m), Exposed (E_m) and Infected (I_m). The total human population, $N_h(t)$, is expressed as

$$N_h(t) = S_h + V_h + E_h + A_h + I_h + T_h + R_h. \tag{2.1}$$

Table 2.1. Model Parameter

Parameter	Description
α_h	Recruitment rate into susceptible humans
α_m	Recruitment rate into susceptible mosquitoes
μ_h	Human natural death rate
μ_m	Mosquito natural death rate
δ_h	Human disease-induced death rate
ω_h	Rate of loss of immunity of recovered humans
β_{hm}	Probability of mosquitoes becoming infected
β_{mh}	Probability of humans becoming infected
ν_h	Vaccine uptake rate
ϵ	Contact rate of mosquito to human
ξ_h	Vaccine waning
σ_h	Vaccine efficacy
ϑ_h	Transition rate from exposed to asymptomatic individuals
κ_h	Transition rate from exposed to infected individuals
κ_m	Transition rate from exposed to infected mosquitoes
τ_h	Transition rate from asymptomatic to infected individuals
φ_h	Transition rate from asymptomatic to recovered individuals
γ_h	Transition rate from infected to treated individuals
η	Drug efficacy
ρ_h	Recovery rate

Similarly, the total mosquito population, $N_m(t)$, is given by

$$N_m(t) = S_m + E_m + I_m. \tag{2.2}$$

The forces of infection λ_h and λ_m are defined as

$$\lambda_h = \frac{\beta_{hm}\epsilon I_m}{N_h} \quad \text{and} \quad \lambda_m = \frac{\beta_{mh}\epsilon I_h}{N_h}$$

where β_{hm} represents the probability of effective transmission of malaria from infected humans to susceptible mosquitoes as a result of contact rate of mosquito to human given by ϵ. Similarly, β_{mh} denotes the probability of effective transmission of malaria from infected mosquitoes to susceptible humans.

2.1. Model Assumptions

1. **Homogeneity of the Populations**: The human population is homogeneously mixed. This implies that there is an equal chance of interaction amongst individuals in the population. This assumption also applies to the vector population, implying random and uniform interactions between mosquitoes.
2. **Vaccination and Immunity**: Malaria vaccines reduce the likelihood of susceptible individuals becoming infected or transitioning to other states of infection. It is noted that since the vaccine is not 100% efficacious, a small proportion of the vaccinated individuals will transit to other state of the infection. Recovered humans have partial immunity, which wanes over time, transitioning them back to the susceptible population.
3. **Transmission Assumption**: Malaria is transmitted from infected humans and mosquitoes to susceptible humans.
4. **Natural Death**: All individuals within the human and vector populations, regardless of their compartmental classification, are subject to natural mortality. However, only humans within the infected and treated compartments experience an additional disease-induced mortality rate.
5. **No Recovery for Infected Mosquitoes**: Infected mosquitoes do not undergo recovery from the disease; therefore, they remain infectious for the entirety of their lifespan, unless mortality occurs due to natural or disease-induced factors.

The flowchart for the proposed model dynamics is as given below:

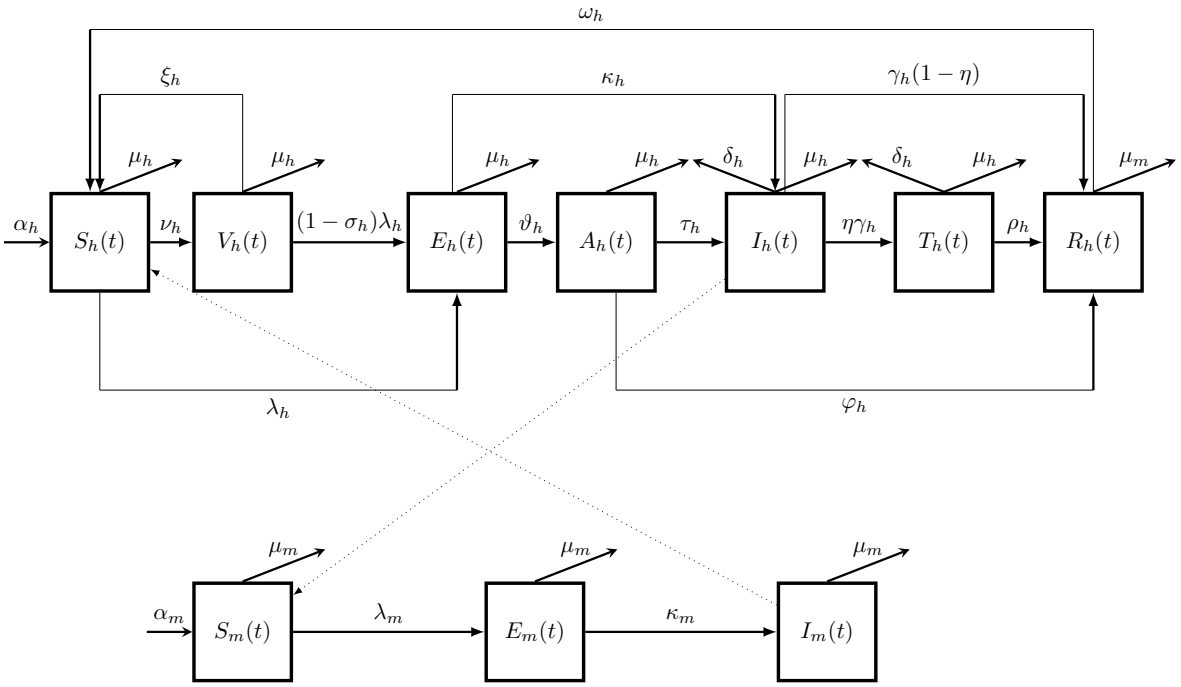

The model is represented by the non-linear system of ODEs below:

$$\begin{cases} \frac{dS_h}{dt} = \alpha_h + w_h R_h + \xi_h V_h - \nu_h S_h - \lambda_h S_h - \mu_h S_h \\ \frac{dV_h}{dt} = \nu_h S_h - (1-\sigma_h)\lambda_h V_h - \xi_h V_h - \mu_h V_h \\ \frac{dE_h}{dt} = \lambda_h S_h + (1-\sigma_h)\lambda_h V_h - \vartheta_h E_h - \kappa_h E_h - \mu_h E_h \\ \frac{dA_h}{dt} = \vartheta_h E_h - \tau_h A_h - \varphi_h A_h - \mu_h A_h \\ \frac{dI_h}{dt} = \kappa_h E_h + \tau_h A_h - \gamma_h I_h - (\delta_h + \mu_h) I_h \\ \frac{dT_h}{dt} = \eta\gamma_h I_h - \rho_h T_h - (\delta_h + \mu_h) T_h \\ \frac{dR_h}{dt} = \varphi_h A_h + \gamma_h(1-\eta) I_h + \rho_h T_h - w_h R_h - \mu_h R_h \\ \frac{dS_m}{dt} = \alpha_m - \lambda_m S_m - \mu_m S_m \\ \frac{dE_m}{dt} = \lambda_m S_m - \kappa_m E_m - \mu_m E_m \\ \frac{dI_m}{dt} = \kappa_m E_m - \mu_m I_m \end{cases} \tag{2.3}$$

with the initial conditions

$$S_h(t) > 0, V_h(t) \geq 0, E_h(t) \geq 0, A_h(t) \geq 0, I_h(t) > 0, T_h(t) \geq 0, R_h(t), S_m(t) > 0, E_m(t) \geq 0, I_m(t) > 0. \tag{2.4}$$

2.1.1. Positivity of solutions The positivity of solutions for the malaria system 2.3 will be verified for all non-negative initial conditions of the compartments at $t > 0$. The proof demonstrating the non-negativity of the solutions for all state variables of system 2.3 is presented below for all $t > 0$,

Theorem 1
Given that the initial conditions 2.4 of system 2.3, there exists $\big(S_h(0), V_h(0), E_h(0), A_h(0), I_h(0), T_h(0), R_h(0), S_m(0), E_m(0), I_m(0) > 0\big)$: $(0, \text{inf}) \longrightarrow (0, \text{inf})$ which solves system 2.3.

Proof
Assume that $\hat{t} = \sup\{S_h(0) > 0, V_h(0) > 0, E_h(0) > 0, A_h(0) > 0, I_h(0) > 0, T_h(0) > 0, R_h(0) > 0, S_m(0) > 0, E_m(0) > 0, I_m(0) > 0$, this implies that $\hat{t} > 0$ □

It follows that

$$\frac{dS_h(t)}{dt} \geq -\left(\nu_h + \mu_h + \lambda_h\right) S_h \tag{2.5}$$

Employing separation of variables, it follows that

$$\frac{dS_h(t)}{S_h(t)} \geq -\left(\nu_h + \mu_h + \lambda_h\right) dt \tag{2.6}$$

Upon integrating 2.6 and using the initial condition, we arrive at

$$S_h(t) \geq S_h(0) e^{-\left((\nu_h+\mu_h)t + \int_0^t \lambda_h(\zeta)d\zeta\right)} \geq 0, \quad \forall\, t \geq 0.$$

Similarly,

$$\begin{cases} V_h(t) \geq V_h(0) e^{-(\xi_h+\mu_h)t + \int_0^t (1-\sigma_h)\lambda_h(\zeta)d\zeta} \geq 0, \quad \forall\, t \geq 0, \\ E_h(t) \geq E_h(0) e^{-(\vartheta_h+\kappa_h+\mu_h)t} \geq 0, \quad \forall\, t \geq 0, \\ A_h(t) \geq A_h(0) e^{-(\tau_h+\varphi_h+\mu_h)t} \geq 0, \quad \forall\, t \geq 0, \\ I_h(t) \geq I_h(0) e^{-(\gamma_h+\delta_h+\mu_h)t} \geq 0, \quad \forall\, t \geq 0, \\ T_h(t) \geq T_h(0) e^{-(\rho_h+\delta_h+\mu_h)t} \geq 0, \quad \forall\, t \geq 0, \\ R_h(t) \geq R_h(0) e^{-(w_h+\mu_h)t} \geq 0, \quad \forall\, t \geq 0, \\ S_m(t) \geq S_m(0) e^{-(\mu_m)t + \int_0^t \lambda_m(\zeta)d\zeta} \geq 0, \quad \forall\, t \geq 0, \\ E_m(t) \geq E_m(0) e^{-(\kappa_m+\mu_m)t} \geq 0, \quad \forall\, t \geq 0, \\ I_m(t) \geq I_m(0) e^{-\mu_m t} \geq 0, \quad \forall\, t \geq 0, \end{cases}$$

2.1.2. The Invariant Region The invariant region (Ω) associated with system 2.3 is defined as the region within the state space where the model variables, representing population sizes or concentrations, remain non-negative and bounded, ensuring biological feasibility. To construct this invariant region, it is necessary to determine the subset of the state space where the population sizes remain constrained within biologically meaningful limits and exhibit bounded behavior over time.

Theorem 2
Let $S_h(t), V_h(t), E_h(t), A_h(t), I_h(t), T_h(t), R_h(t), S_m(t), E_m(t), I_m(t)$ be the solutions of system 2.3 with initial conditions $(S_h(0), V_h(0), E_h(0), A_h(0), I_h(0), T_h(0), R_h(0), S_m(0), E_m(0), I_m(0))$. The compact set

$$\Omega = \{(S_h(t), V_h(t), E_h(t), A_h(t), I_h(t), T_h(t), R_h(t), S_m(t), E_m(t), I_m(t)) \in \mathbb{R}_+^{10} : N_h \leq \frac{\alpha_h}{\mu_h}, \quad N_m \leq \frac{\alpha_m}{\mu_m}\} \tag{2.7}$$

attracts all solutions in $\mathbb{R}_+^{10}$ and is positively invariant.

Proof
We define a region within the non-negative orthant $\mathbb{R}_+^{10}$ that contains uniformly bounded solutions to the model 2.3, encompassing the human and mosquito populations. In view of these populations given in equations 2.1 and 2.2 respectively, we have

$$\frac{dN_h}{dt} = \frac{dS_h}{dt} + \frac{dV_h}{dt} + \frac{dE_h}{dt} + \frac{dA_h}{dt} + \frac{dI_h}{dt} + \frac{dT_h}{dt} + \frac{dR_h}{dt} \tag{2.8}$$

and

$$\frac{dN_m}{dt} = \frac{dS_m}{dt} + \frac{dE_m}{dt} + \frac{dI_m}{dt} \tag{2.9}$$

In the context of model 2.3, equation 2.8 becomes

$$\frac{dN_h}{dt} = \alpha_h - \mu_h N_h - \delta_h I_h - \delta_h T_h \leq \alpha_h - \mu_h N_h \tag{2.10}$$

Equation 2.10 implies that $\frac{dN_h}{dt} \leq 0$. Thus, the region Ω represents a set that is positively invariant. By solving equation 2.10, we derive

$$N_h(t) \to \tfrac{\alpha_h}{\mu_h} \; as \; t \to \infty$$

Thus, $N_h(t) \in [0, \frac{\alpha_h}{\mu_h}]$.
Similarly; $N_m(t) \in [0, \frac{\alpha_m}{\mu_m}]$. □

2.2. The Equilibrium Points

2.2.1. The Disease-Free Equilibrium Point (DFE): At the DFE, no infection or recovery occurs. Consequently, all the compartments associated with infection: $E_h, A_h, I_h, T_h, R_h, E_m, I_m$ are set to zero in model 2.3. By solving the remaining compartments at equilibrium, we derive the DFE as

$$\varepsilon^0 = \left(S_h^0 = \frac{\alpha_h(\xi_h+\mu_h)}{\mu_h(\xi_h+\nu_h+\mu_h)}, V_h^0 = \frac{\alpha_h\nu_h}{\mu_h(\xi_h+\nu_h+\mu_h)}, E_h^0 = 0, A_h^0 = 0, I_h^0 = 0, T_h^0 = 0, R_h^0 = 0, S_m^0 = \frac{\alpha_m}{\mu_m}, E_m^0 = 0, I_m^0 = 0\right). \tag{2.11}$$

2.3. Local Asymptomatic Stability Analysis

2.3.1. The Effective Reproduction Number In a completely susceptible population, the effective reproduction number, $\mathcal{R}_e$, is defined as the expected number of secondary cases generated by an infected individual during its infectious period. It corresponds to the spectral radius of the next generation matrix $G = FV^{-1}$ associated with model 2.3, where:

$$F = \begin{pmatrix} 0 & 0 & 0 & 0 & 0 & \frac{\beta_{hm}\epsilon\, S_h + (1-\sigma_h)\beta_{hm}\epsilon\, V_h}{N_h} \\ 0 & 0 & 0 & 0 & 0 & 0 \\ 0 & 0 & 0 & 0 & 0 & 0 \\ 0 & 0 & 0 & 0 & 0 & 0 \\ 0 & 0 & \frac{\beta_{mh}\epsilon\, S_m}{N_h} & 0 & 0 & 0 \\ 0 & 0 & 0 & 0 & 0 & 0 \end{pmatrix} \tag{2.12}$$

$$V = \begin{pmatrix} \vartheta_h + \kappa_h + \mu_h & 0 & 0 & 0 & 0 & 0 \\ -\vartheta_h & \tau_h + \psi_h + \mu_h & 0 & 0 & 0 & 0 \\ -\kappa_h & -\tau_h & \gamma_h + \delta_h + \mu_h & 0 & 0 & 0 \\ 0 & 0 & -\eta\,\gamma_h & \rho_h + \delta_h + \mu_h & 0 & 0 \\ 0 & 0 & 0 & 0 & \kappa_m + \mu_m & 0 \\ 0 & 0 & 0 & 0 & -\kappa_m & \mu_m \end{pmatrix} \tag{2.13}$$

where $k_1 = \nu_h + \mu_h$, $k_2 = \sigma_h + \xi_h + \mu_h$, $k_3 = \vartheta_h + \kappa_h + \mu_h$, $k_4 = \tau_h + \varphi_h + \mu_h$, $k_5 = \gamma_h + \delta_h + \mu_h$, $k_6 = \rho_h + \delta_h + \mu_h$, $k_7 = w_h + \mu_h$, $k_8 = \mu_m$, $k_9 = \kappa_m + \mu_m$ and $k_{10} = \mu_m$. Hence, the $\mathcal{R}_e$ for the system 2.3 is given by

$$\mathcal{R}_e = \rho(FV^{-1}) = \sqrt{\mathcal{R}_h\mathcal{R}_m} = \sqrt{\frac{\beta_{mh}\,\beta_{hm}\,\alpha_m\,\kappa_m\,\mu_h\left(\vartheta_h\tau_h + k_4\kappa_h\right)\left((\sigma_h-1)\nu_h - \mu_h - \xi_h\right)\epsilon^2}{\alpha_h\,k_3^2k_4^2k_5^2\,k_9\,\mu_m^2\,(\xi_h+\nu_h+\mu_h)^2}} \tag{2.14}$$

where

$$\mathcal{R}_h = \frac{\beta_{mh}\,\mu_h\,\left(\vartheta_h\tau_h + k_4\kappa_h\right)\epsilon}{\alpha_h\,k_3^2\,k_4^2\,k_5^2\,(\xi_h+\nu_h+\mu_h)^2} \tag{2.15}$$

$$\mathcal{R}_m = \frac{\beta_{hm}\,\alpha_m\,\kappa_m\,k_9\,\left((\sigma_h-1)\nu_h-\mu_h-\xi_h\right)\epsilon}{\mu_m^2\,k_9} \tag{2.16}$$

Therefore, malaria can be completely eliminated from the population if $\mathcal{R}_e < 1$, as stated in the following theorem:

2.4. Stability Analysis of the Disease free Equilibrium

Theorem 3
The DFE, $\mathcal{E}^0$, of model (2.3) and represented by Equation (2.11), will be locally-asymptotically stable (LAS) when $\mathcal{R}_e < 1$, and unstable when $\mathcal{R}_e > 1$.

Proof
To prove Theorem (3), we derive the Jacobian matrix of model (2.3) at $\mathcal{E}^0$ as

$$J(\mathcal{E}^0) = \begin{pmatrix}
-k_1 & \xi_h & 0 & 0 & 0 & 0 & \omega_h & 0 & 0 & -\frac{\beta_{hm}\epsilon\,\alpha_h(\xi_h+\mu_h)(\nu_h+\mu_h)(\sigma_h+\xi_h+\mu_h)}{\mu_h(\xi_h+\nu_h+\mu_h)\alpha_h(\sigma_h+\xi_h+\mu_h+\nu_h)} \\
\nu_h & -k_2 & 0 & 0 & 0 & 0 & 0 & 0 & 0 & \frac{(-1+\sigma_h)\beta_{hm}\epsilon\,\nu_h(\nu_h+\mu_h)(\sigma_h+\xi_h+\mu_h)}{\mu_h(\xi_h+\nu_h+\mu_h)(\sigma_h+\xi_h+\mu_h+\nu_h)} \\
0 & 0 & -k_3 & 0 & 0 & 0 & 0 & 0 & 0 & -\frac{(\nu_h+\mu_h)\epsilon\,(\sigma_h+\xi_h+\mu_h)(-\alpha_h(\xi_h+\mu_h)+(-1+\sigma_h)\alpha_h\nu_h)\beta_{hm}}{\mu_h(\xi_h+\nu_h+\mu_h)\alpha_h(\sigma_h+\xi_h+\mu_h+\nu_h)} \\
0 & 0 & \vartheta_h & -k_4 & 0 & 0 & 0 & 0 & 0 & 0 \\
0 & 0 & \kappa_h & \tau_h & -k_5 & 0 & 0 & 0 & 0 & 0 \\
0 & 0 & 0 & 0 & \eta\,\gamma_h & -k_6 & 0 & 0 & 0 & 0 \\
0 & 0 & 0 & \varphi_h & \gamma_h\,(1-\eta) & \rho_h & -k_7 & 0 & 0 & 0 \\
0 & 0 & 0 & 0 & -\frac{\beta_{mh}\epsilon\,\alpha_m(\nu_h+\mu_h)(\sigma_h+\xi_h+\mu_h)}{\mu_m\alpha_h(\sigma_h+\xi_h+\mu_h+\nu_h)} & 0 & 0 & -k_8 & 0 & 0 \\
0 & 0 & 0 & 0 & \frac{\beta_{mh}\epsilon\,\alpha_m(\nu_h+\mu_h)(\sigma_h+\xi_h+\mu_h)}{\mu_m\alpha_h(\sigma_h+\xi_h+\mu_h+\nu_h)} & 0 & 0 & 0 & -k_9 & 0 \\
0 & 0 & 0 & 0 & 0 & 0 & 0 & 0 & \kappa_m & -k_{10}
\end{pmatrix} \tag{2.17}$$

The first five eigenvalues of the Jacobian matrix (2.17) are given as

$$\lambda_i^* = \begin{pmatrix} -k_1 \\ -k_2 \\ -k_6 \\ -k_7 \\ -k_8 \end{pmatrix} \tag{2.18}$$

The following sub-matrix can be used to obtain the remaining eigenvalues

$$\mathcal{J} = \begin{pmatrix}
-k_3 & 0 & 0 & 0 & -\frac{(\nu_h+\mu_h)\epsilon\,(\sigma_h+\xi_h+\mu_h)(-\alpha_h(\xi_h+\mu_h)+(-1+\sigma_h)\alpha_h\nu_h)\beta_{hm}}{\mu_h(\xi_h+\nu_h+\mu_h)\alpha_h(\sigma_h+\xi_h+\mu_h+\nu_h)} \\
\vartheta_h & -k_4 & 0 & 0 & 0 \\
\kappa_h & \tau_h & -k_5 & 0 & 0 \\
0 & 0 & \frac{\beta_{mh}\epsilon\,\alpha_m(\nu_h+\mu_h)(\sigma_h+\xi_h+\mu_h)}{\mu_m\alpha_h(\sigma_h+\xi_h+\mu_h+\nu_h)} & -k_9 & 0 \\
0 & 0 & 0 & \kappa_m & -k_{10}
\end{pmatrix} \tag{2.19}$$

The chareacteristic equation of matrix 2.19 is given as

$$\alpha_{\mathbf{5}}\lambda^5 + \alpha_{\mathbf{4}}\lambda^4 + \alpha_{\mathbf{3}}\lambda^3 + \alpha_{\mathbf{2}}\lambda^2 + \alpha_{\mathbf{1}}\lambda + \alpha_0 = 0 \tag{2.20}$$

where
$\alpha_{\mathbf{5}} = 1$

$$(k_{10}k_3k_4k_5 + k_{10}k_3k_4k_9 + k_{10}k_3k_5k_9 + k_{10}k_4k_5k_9 + k_3k_4k_5k_9) - R_e^2 \tag{2.21}$$

$$\alpha_0 = \mu_m k_3 k_4 k_5 k_9 (1 - R_e^2) \tag{2.22}$$

Based on the Routh-Hurwitz criterion [49], for the matrix $\mathcal{J}$ to have all eigenvalues real and negative, it must satisfy the conditions

1. all coefficients α_i are positive, and
2. the Hurwitz matrices H_i are positive for $i = 2, 3, 4$ and 5.

It is obvious that α_2, α_3, α_4, α_5 are positive since all the associated term are positive.If the $R_e < 1$, then equations 2.21 and 2.22, imply that $\alpha_0 > 0$. and $\alpha_1 > 0$. This shows that the DFE is stable since $R_e < 1$ and it reveals that malaria infection can be curtail. Given the follwoing Hurwitz matrices from the characteristic equation 2.20: $H_1 = \alpha_4 > 0$, $H_2 = det \begin{pmatrix} \alpha_4 & \alpha_2 \\ \alpha_5 & \alpha_3 \end{pmatrix} > 0$,$H_3 = det \begin{pmatrix} \alpha_4 & \alpha_2 & \alpha_0 \\ \alpha_5 & \alpha_3 & \alpha_1 \\ 0 & \alpha_4 & \alpha_2 \end{pmatrix} > 0$, $H_4 = det \begin{pmatrix} \alpha_4 & \alpha_2 & \alpha_0 & 0 \\ \alpha_5 & \alpha_3 & \alpha_1 & 0 \\ 0 & \alpha_4 & \alpha_2 & \alpha_0 \\ 0 & \alpha_5 & \alpha_3 & \alpha_1 \end{pmatrix} > 0$,

$H_5 = det \begin{pmatrix} \alpha_4 & \alpha_2 & \alpha_0 & 0 & 0 \\ \alpha_5 & \alpha_3 & \alpha_1 & 0 & 0 \\ 0 & \alpha_4 & \alpha_2 & \alpha_0 & 0 \\ 0 & \alpha_5 & \alpha_3 & \alpha_1 & 0 \\ 0 & 0 & \alpha_4 & \alpha_2 & \alpha_0 \end{pmatrix} > 0.$

Since $H_i > 0, \forall\ i = 1, \ldots, 5$, this confirms the stability of the system. When $\mathcal{R}_e < 1$, the eigenvalues of matrix (2.19) are both real and negative, implying that the DFE, $\mathcal{E}^0$, is LAS. On the other hand, if $\mathcal{R}_e > 1$, the eigenvalues become unstable, resulting in the instability of $\mathcal{E}^0$. Furthermore, by the Poincaré-Lyapunov theorem, since the two conditions above are satisfied and jacobian $J(\mathcal{E}^0)$ has all eigenvalues with negative real parts, as demonstrated in (2.18), $\mathcal{E}^0$ is confirmed to be locally asymptotically stable. □

2.5. Global Asymptotic Stability (GAS)

The Disease-Free Equilibrium (DFE) for global asymptotic stability of system 2.3 is analyzed through the application of the Lyapunov direct method, as outlined in [11, 35, 75]. By constructing an appropriate Lyapunov function, we show that the DFE is GAS if $\mathcal{R}_e < 1$. This ensures that, regardless of the initial conditions, the population will tend to the DFE over time, meaning that the disease will eventually be eradicated in the system:

$$\begin{cases} \frac{dU}{dt} = \mathbf{F}(\mathbf{U}, \mathbf{V}) \\ \frac{dV}{dt} = \mathbf{G}(\mathbf{U}, \mathbf{V}) \end{cases} \tag{2.23}$$

where the uninfected population is denoted by $U = (S_h, V_h, R_h, S_m)$ and $V = (E_h, A_h, I_h, T_h, E_m, I_m)$ represents the infected population. Thus, the point $\mathcal{E}^0 = (U^*, 0)$ is said to be GAS if $\mathcal{R}_e < 1$.

Theorem 4
The DFE is said to be GAS in $\Omega = (S_h(t), V_h(t), E_h(t), A_h(t), I_h(t), T_h(t), R_h(t), S_m(t), E_m(t), I_m(t)) \in \mathbb{R}_+^{10}$ if $\mathcal{R}_e$<1 and the two conditions below are satisfied:

1. C_1: $\frac{dU}{dt} = \mathbf{F}(\mathbf{U}, \mathbf{0})$, $\mathcal{E}^0$ is GAS
2. C_2: $\mathbf{G}(\mathbf{X}, \mathbf{Y}) = AV - G^*(U, V)$, $G^*(U, V) \geq 0$ for $(U, V) \in \Omega$

Proof
For C_1, model 2.3 gives

$$\mathbf{F}(\mathbf{U}, \mathbf{0}) = \begin{cases} \alpha_h + w_h R_h + \xi_h V_h - \nu_h S_h - \mu_h S_h \\ \nu_h S_h - \xi_h V_h - \mu_h V_h \\ \vartheta_h A_h + \gamma_h (1 - \eta) I_h + \rho_h T_h - w_h R_h - \mu_h R_h \\ \alpha_m - \mu_m S_m \end{cases} \tag{2.24}$$

Thus, $\mathcal{E}^0 = \left(S_h^0 = \frac{\alpha_h(\xi_h+\mu_h)}{\mu_h(\xi_h+\nu_h+\mu_h)}, V_h^0 = \frac{\alpha_h\nu_h}{\mu_h(\xi_h+\nu_h+\mu_h)}, E_h^0 = 0, A_h^0 = 0, I_h^0 = 0, T_h^0 = 0, R_h^0 = 0, S_m^0 = \frac{\alpha_m}{\mu_m}, E_m^0 = 0, I_m^0 = 0\right)$ is GAS for $\frac{dU}{dt} = \mathbf{F}(\mathbf{U}, \mathbf{0})$. By adopting the technique of integrating factor, we have

$$\frac{dS_h}{dt} + (\nu_h + \mu_h)S_h = \alpha_h + \xi_h V_h + w_h R_h$$

$$\frac{d}{dt}\left(S_h e^{(\nu_h+\mu_h)t}\right) = \alpha_h e^{(\nu_h+\mu_h)t} + (\xi_h V_h + \omega_h R_h)e^{(\nu_h+\mu_h)t}$$

$$S_h e^{(\nu_h+\mu_h)t} = \alpha_h \int e^{(\nu_h+\mu_h)t}dt + \int (\xi_h V_h + \omega_h R_h)e^{(\nu_h+\mu_h)t}dt$$

$$S_h e^{(\nu_h+\mu_h)t} = \frac{\alpha_h e^{(\nu_h+\mu_h)t}}{(\nu_h+\mu_h)} + \int (\xi_h V_h + \omega_h R_h)e^{(\nu_h+\mu_h)t}dt$$

$$S_h = \frac{\alpha_h}{(\nu_h+\mu_h)} + \frac{\xi_h V_h + \omega_h R_h}{\nu_h+\mu_h}e^{-(\nu_h+\mu_h)t} - \int \frac{\xi_h V_h^{'} + \omega_h R_h^{'}}{\nu_h+\mu_h}e^{(\nu_h+\mu_h)t}dt$$

Hence, $S_h(t) \to \frac{\alpha_h}{(\nu_h+\mu_h)}$ as $t \to \infty$.

Using a similar approach, $S_m(t) \to \frac{\alpha_m}{\mu_m}$ as $t \to \infty$. Thus, this implies that equation 2.24 is globally convergent in Ω

For C_2:

$$\mathbf{G}(\mathbf{X}, \mathbf{Y}) = \begin{cases} \lambda_h S_h + (1-\sigma_h)\lambda_h V_h - \vartheta_h E_h - \kappa_h E_h - \mu_h E_h \\ \vartheta_h E_h - \tau_h A_h - \varphi_h A_h - \mu_h A_h \\ \kappa_h E_h + \tau_h A_h - \gamma_h I_h - (\delta_h + \mu_h)I_h \\ \eta\gamma_h I_h - \rho_h T_h - (\delta_h + \mu_h)T_h \\ \lambda_m S_m - \kappa_m E_m - \mu_m E_m \\ \kappa_m E_m - \mu_m I_m \end{cases} \tag{2.25}$$

$$= AV - G^*(U, V)$$

where

$$A = \begin{pmatrix} -\vartheta_h - \kappa_h - \mu_h & 0 & 0 & 0 & 0 & 0 \\ \vartheta_h & -\tau_h - \varphi_h - \mu_h & 0 & 0 & 0 & 0 \\ \kappa_h & \tau_h & -\gamma_h - \delta_h - \mu_h & 0 & 0 & 0 \\ 0 & 0 & \eta\gamma_h & -\rho_h - \delta_h - \mu_h & 0 & 0 \\ 0 & 0 & 0 & 0 & -\kappa_m - \mu_m & 0 \\ 0 & 0 & 0 & 0 & \kappa_m & -\mu_m \end{pmatrix}$$

and

$$\mathbf{G}^*(\mathbf{U}, \mathbf{V}) = \begin{pmatrix} -(\lambda_h S_h + (1-\sigma_h)\lambda_h V_h) \\ 0 \\ 0 \\ 0 \\ -\lambda_m S_m \\ 0 \end{pmatrix}$$

Condition C_2 is not satisfied since $\mathbf{G}^*(\mathbf{U}, \mathbf{V}) \leq 0$. Hence, for $\mathcal{R}_e < 1$, $\mathcal{E}^0 = (U^*, 0)$ may not be Globally Asymptomatically Stable. □

2.5.1. The Endemic Equilibrium Point (EEP) All disease states in model 2.3 are considered positive at the EEP. In view of this, when S_h^{**} in the model 2.3 is positive, then a unique EEP exists. This is equivalent to having $\mathcal{R}_e > 1$. Thus, the EEP is defined as $\mathcal{E}^1 = (S_h^{**}, V_h^{**}, E_h^{**}, A_h^{**}, I_h^{**}, T_h^{**}, R_h^{**}, S_m^{**}, E_m^{**}, I_m^{**})$ and it satisfies $\frac{dS_h}{dt} = \frac{dV_h}{dt} = \frac{dE_h}{dt} = \frac{dA_h}{dt} = \frac{dI_h}{dt} = \frac{dT_h}{dt} = \frac{dR_h}{dt} = \frac{dS_m}{dt} = \frac{dE_m}{dt} = \frac{dI_m}{dt} = 0$. In view of the complex nature of system 2.3, all the state variables are represented in terms of the forces of infection λ_h^{**} and λ_m^{**} at the steady state. Accordingly,

$$
\begin{cases}
S_h^{*}* = \dfrac{k_6 k_5 \alpha_h k_4 \left((\sigma_h - 1)\lambda_h^{**} - k_2\right) k_7 k_3}{k_6 \lambda_h^{**} (k_4\kappa_h + \psi_h\tau_h) w_h \left((\sigma_h - 1)\lambda_h^{**} + \nu_h\sigma_h - \nu_h - k_2\right)\gamma_h(1-\eta) + A(\sigma_h - 1)\lambda_h^{**2} + B\lambda_h^{**} - k_3k_4k_5k_6k_7(-k_1k_2 + \nu_h\xi_h)} \\
V_h^{*}* = \dfrac{\nu_h k_3 k_4 k_6 k_5 k_7 \alpha_h}{k_6 \lambda_h^{**} (k_4\kappa_h + \psi_h\tau_h) w_h \left((\sigma_h - 1)\lambda_h^{**} + \nu_h\sigma_h - \nu_h - k_2\right)\gamma_h(1-\eta) + A(\sigma_h - 1)\lambda_h^{**2} + B\lambda_h^{**} - k_3k_4k_5k_6k_7(-k_1k_2 + \nu_h\xi_h)} \\
E_h^{*}* = \dfrac{k_4 \lambda_h^{**} \left(k_2 + \lambda_h^{**} + \nu_h - \lambda_h^{**}\sigma_h - \nu_h\sigma_h\right) k_6 k_5 k_7 \alpha_h}{k_6 \lambda_h^{**} (k_4\kappa_h + \psi_h\tau_h) w_h \left((\sigma_h - 1)\lambda_h^{**} + \nu_h\sigma_h - \nu_h - k_2\right)\gamma_h(1-\eta) + A(\sigma_h - 1)\lambda_h^{**2} + B\lambda_h^{**} - k_3k_4k_5k_6k_7(-k_1k_2 + \nu_h\xi_h)} \\
A_h^{*}* = \dfrac{\lambda_h^{**}\psi_h \left(k_2 + \lambda_h^{**} + \nu_h - \lambda_h^{**}\sigma_h - \nu_h\sigma_h\right) k_6 k_5 k_7 \alpha_h}{k_6 \lambda_h^{**} (k_4\kappa_h + \psi_h\tau_h) w_h \left((\sigma_h - 1)\lambda_h^{**} + \nu_h\sigma_h - \nu_h - k_2\right)\gamma_h(1-\eta) + A(\sigma_h - 1)\lambda_h^{**2} + B\lambda_h^{**} - k_3k_4k_5k_6k_7(-k_1k_2 + \nu_h\xi_h)} \\
I_h^{*}* = \dfrac{(k_4\kappa_h + \psi_h\tau_h)\lambda_h^{**} \left(k_2 + \lambda_h^{**} + \nu_h - \lambda_h^{**}\sigma_h - \nu_h\sigma_h\right) k_6 k_7 \alpha_h}{k_6 \lambda_h^{**} (k_4\kappa_h + \psi_h\tau_h) w_h \left((\sigma_h - 1)\lambda_h^{**} + \nu_h\sigma_h - \nu_h - k_2\right)\gamma_h(1-\eta) + A(\sigma_h - 1)\lambda_h^{**2} + B\lambda_h^{**} - k_3k_4k_5k_6k_7(-k_1k_2 + \nu_h\xi_h)} \\
T_h^{*}* = \dfrac{\eta\gamma_h(k_4\kappa_h + \psi_h\tau_h)\lambda_h^{**} \left(k_2 + \lambda_h^{**} + \nu_h - \lambda_h^{**}\sigma_h - \nu_h\sigma_h\right) k_7 \alpha_h}{k_6 \lambda_h^{**} (k_4\kappa_h + \psi_h\tau_h) w_h \left((\sigma_h - 1)\lambda_h^{**} + \nu_h\sigma_h - \nu_h - k_2\right)\gamma_h(1-\eta) + A(\sigma_h - 1)\lambda_h^{**2} + B\lambda_h^{**} - k_3k_4k_5k_6k_7(-k_1k_2 + \nu_h\xi_h)} \\
R_h^{*}* = \dfrac{\lambda_h^{**}\alpha_h \left(k_6(k_4\kappa_h + \psi_h\tau_h)\gamma_h(1-\eta) + \phi_h\psi_h k_5 k_6 + \eta\rho_h\gamma_h(k_4\kappa_h + \psi_h\tau_h)\right)\left((\sigma_h - 1)\lambda_h^{**} + \nu_h\sigma_h - \nu_h - k_2\right)}{k_6 \lambda_h^{**} (k_4\kappa_h + \psi_h\tau_h) w_h \left((\sigma_h - 1)\lambda_h^{**} + \nu_h\sigma_h - \nu_h - k_2\right)\gamma_h(1-\eta) + A(\sigma_h - 1)\lambda_h^{**2} + B\lambda_h^{**} - k_3k_4k_5k_6k_7(-k_1k_2 + \nu_h\xi_h)} \\
S_m^{*}* = \dfrac{\alpha_m}{\lambda_m^{**} + \mu_m} \\
E_m^{**} = \dfrac{\lambda_m^{**}\alpha_m}{k_9\left(\lambda_m^{**} + \mu_m\right)} \\
I_m^{*}* = \dfrac{\kappa_m\lambda_m^{**}\alpha_m}{\mu_m k_9\left(\lambda_m^{**} + \mu_m\right)}
\end{cases}
\tag{2.26}
$$

where $A = (\phi_h\psi_h k_5 k_6 + \eta\rho_h\gamma_h(k_4\kappa_h + \psi_h\tau_h))w_h - k_3k_4k_5k_6k_7$ and
$B = (\nu_h\sigma_h - k_2 - \nu_h)(\phi_h\psi_h k_5 k_6 + \eta\rho_h\gamma_h(k_4\kappa_h + \psi_h\tau_h))w_h - k_3k_4k_5k_6k_7(k_1\sigma_h - k_1 - k_2)$ with the forces of infections defined by

$$
\lambda_h^{**} = \frac{\beta_{hm}\epsilon I_m^{**}}{N_h^{**}} \quad \text{and} \quad \lambda_m^{**} = \frac{\beta_{mh}\epsilon I_h^{**}}{N_h^{**}}.
$$

Theorem 5
The EEP, denoted as $\mathcal{E}^1$, will be GAS whenever $\mathcal{R}_e > 1$.

Proof
The Invariance Principle of Lyapunov-Lasalle, which entails examining the Lyapunov candidate function for $\mathcal{E}^1$, is used to prove the theorem.

$$
\begin{aligned}
V = &\frac{1}{2}\left(S_h - S_h^{**}\right)^2 + \frac{1}{2}\left(V_h - V_h^{**}\right)^2 + \frac{1}{2}\left(E_h - E_h^{**}\right)^2 + \frac{1}{2}\left(A_h - A_h^{**}\right)^2 + \frac{1}{2}\left(I_h - I_h^{**}\right)^2 + \frac{1}{2}\left(T_h - T_h^{**}\right)^2 + \\
&\frac{1}{2}\left(R_h - R_h^{**}\right)^2 + \frac{1}{2}\left(S_m - S_m^{**}\right)^2 + \frac{1}{2}\left(E_m - E_m^{**}\right)^2 + \frac{1}{2}\left(I_m - I_m^{**}\right)^2
\end{aligned}
\tag{2.27}
$$

Taking the derivative of (4.5),

$$\begin{aligned}
\dot{V} =&\big(S_h - S_h^{**}\big)\dot{S}_h + \big(V_h - V_h^{**}\big)\dot{V}_h + \big(E_h - E_h^{**}\big)\dot{E}_h + \big(A_h - A_h^{**}\big)\dot{A}_h + \big(I_h - I_h^{**}\big)\dot{I}_h + \big(T_h - T_h^{**}\big)\dot{T}_h \\
&+\big(R_h - R_h^{**}\big)\dot{R}_h + \big(S_m - S_m^{**}\big)\dot{S_m} + \big(E_m - E_m^{**}\big)\dot{E_m} + \big(I_m - I_m^{**}\big)\dot{I_m}\text{`} \\
=&\Bigg(\big(\alpha_h + w_h R_h + \xi_h V_h)S_h + \big(\nu_h + \lambda_h + \mu_h)S_h^{**} S_h + \nu_h S_h V_h + \big((1-\sigma_h)\lambda_h + \xi_h + \mu_h)V_h^{**} V_h + \\
&\big(\lambda_h S_h + (1-\sigma_h)\lambda_h V_h\big)E_h + \big(\vartheta_h + \kappa_h + \mu_h)E_h^{**} E_h + \vartheta_h E_h A_h + (\tau_h + \varphi_h + \mu_h)A_h^{**} A_h + \\
&\big(\kappa_h E_h + \tau_h A_h\big)I_h + \big(\gamma_h + \delta_h + \mu_h)I_h^{**} I_h + \eta\gamma_h I_h T_h + (\rho_h + \delta_h + \mu_h)T_h^{**} T_h + \\
&(\varphi_h A_h + \gamma_h(1-\eta)I_h + \rho_h T_h)R_h + (w_h + \mu_h)R_h^{**} R_h + \alpha_m S_m + (\lambda_m + \mu_m)S_m^{**} S_m + \lambda_m S_m E_m + \\
&(\kappa_m + \mu_m)E_m^{**} E_m + \kappa_m E_m I_m + \mu_m I_m^{**} I_m \Bigg) - \\
&\Bigg(\big(\nu_h + \lambda_h + \mu_h)S_h + \big(\alpha_h + w_h R_h + \xi_h V_h)S_h^{**} S_h + \big((1-\sigma_h)\lambda_h + \xi_h + \mu_h)V_h + \nu_h S_h V_h^{**} V_h + \\
&\big(\vartheta_h + \kappa_h + \mu_h)E_h + \big(\lambda_h S_h + (1-\sigma_h)\lambda_h V_h\big)E_h^{**} E_h + (\tau_h + \varphi_h + \mu_h)A_h + \vartheta_h E_h A_h^{**} A_h + \\
&\big(\gamma_h + \delta_h + \mu_h\big)I_h + \big(\kappa_h E_h + \tau_h A_h)I_h^{**} I_h + (\rho_h + \delta_h + \mu_h)T_h + \eta\gamma_h I_h T_h^{**} T_h + \\
&(w_h + \mu_h)R_h + (\varphi_h A_h + \gamma_h(1-\eta)I_h + \rho_h T_h)R_h^{**} R_h + (\lambda_m + \mu_m)S_m + \alpha_m S_m^{**} S_m + (\kappa_m + \mu_m)E_m + \\
&\lambda_m S_m E_m^{**} E_m + \mu_m I_m + \kappa_m E_m I_m^{**} I_m \Bigg)
\end{aligned} \tag{2.28}$$

Therefore, the EEP, $\mathcal{E}^1$, is the largest compact invariant set within $\Big\{\big(S_h, V_h, E_h, A_h, I_h, T_h, R_h, S_m, E_m, I_m\big) \in \Omega : V \leq 0\Big\}$. Thus, using the Lyapunov-LaSalle Invariance Principle, it can be shown that all solutions in the set Ω will converge to $\mathcal{E}^1$ as $t \to \infty$ when $\mathcal{R}_e > 1$. As a result, $\mathcal{E}^1$, is GAS. Notably, this discovery has epidemiological significance because it shows that malaria will persist and spread throughout a community as long as $\mathcal{R}_e > 1$.. □

3. Numerical Simulation

The dynamic behavior of the malaria model, which is presented as an initial value problem in 2.3, is examined in this section. Numerical simulations are conducted with ode45 solver on MATLAB. The model is simulated using the following initial conditions:

$$\begin{aligned}
&S_h(0) = 6083.2, \quad V_h(0) = 800, \quad E_h(0) = 0, \quad A_h(0) = 854, \quad I_h(0) = 2000, \\
&T_h(0) = 683.2, \quad R_h(0) = 200, \quad S_m(0) = 46000, \quad E_m(0) = 2500, \quad I_m(0) = 1500.
\end{aligned} \tag{3.1}$$

3.1. Initial Conditions for Malaria Transmission Model

In calibrating the initial conditions for our malaria transmission model, we adopt field-informed assumptions based on prevalence data from endemic settings and consider the ten classes of model 2.3.

3.1.1. Human Population Dynamics: Assuming a total human population of $N_h(0) = 10{,}000$, and a malaria prevalence of $P_h = 0.20$ (20%), we infer an initial infected human population of:

$$I_h(0) = P_h \times N_h(0) = 2000 \text{ individuals.}$$

Recent studies indicate that $57.3\%$of infected individuals are asymptomatic, while the remaining 42.7% are symptomatic [25]. This yields:

$$A_h(0) = 0.573 \times I_h(0) = 1146, \quad I_h^{\text{sym}}(0) = 0.427 \times I_h(0) = 854.$$

In Nigeria, a high proportion of individuals with malaria-like illness receive some form of antimalarial treatment, either through formal health facilities, pharmacies, chemists, herbal remedies, or self-medication at home. Based on national survey data and peer-reviewed studies, it is estimated that approximately 80% of such individuals obtain treatment. This estimate aligns with findings from a national opinion poll reporting that the majority of symptomatic individuals seek treatment through hospitals (41%), chemists (22%), pharmacies (21%), herbal remedies (11%), or over-the-counter drugs (7%) [46], as well as research showing that more than 60% of uncomplicated malaria cases in public health facilities received treatment [27], and among those seeking care, 72% underwent diagnostic testing prior to treatment [19].

$$T_h(0) = 0.80 \times I_h(0) = 683.2.$$

Assuming no individuals are in the exposed class at $t = 0$, we set:

$$E_h(0) = 0.$$

If 10% of the susceptible population has been vaccinated, we initialize the vaccinated class as:

$$V_h(0) = 0.10 \times (N_h(0) - I_h(0)) = 0.10 \times 8000 = 800.$$

Assuming 10% of previously infected individuals have recovered with immunity:

$$R_h(0) = 0.10 \times I_h(0) = 200.$$

The susceptible human population is then obtained by subtraction:

$$\begin{aligned} S_h(0) &= N_h(0) - \left(V_h(0) + E_h(0) + A_h(0) + I_h^{\text{sym}}(0) + T_h(0) + R_h(0)\right) \\ &= 10{,}000 - (2400 + 0 + 1146 + 854 + 683.2 + 200) = 4483.2. \end{aligned} \tag{3.2}$$

3.1.2. Mosquito Population Dynamics: For the mosquito vector, we assume an initial population of $N_m(0) = 50{,}000$ with an average of patent infection prevalence of 3% [3, 16, 29, 50, 67]. This results in:

$$I_m(0) = P_m \times N_m(0) = 1500 \text{ infected mosquitoes.}$$

Assuming 5% of mosquitoes are in the exposed (latent) stage:

$$E_m(0) = 0.05 \times N_m(0) = 2500.$$

The susceptible mosquito population is:

$$S_m(0) = N_m(0) - (E_m(0) + I_m(0)) = 50{,}000 - (2500 + 1500) = 46{,}000.$$

Parameter Estimation for Malaria Transmission Dynamics

To ensure validity and realism in the development of a malaria transmission model that is biologically plausible, thorough parameter estimate is necessary. Prior modeling research and empirical data are employed to estimate the model parameter values.

Based on Nigeria's average life expectancy of 54.4 years from 2015 to 2024 [74, 81, 77], we calculate human natural mortality rate as:

$$\mu_h = \frac{1}{54.4 \times 365} = 5.04 \times 10^{-5}\,\text{d}^{-1}$$

For a baseline population $N_h(0) = 10{,}000$, the human recruitment rate is:

$$\alpha_h = \mu_h N_h(0) = (5.04 \times 10^{-5})(10{,}000) = 0.504 \,\text{individuals d}^{-1},$$

ensuring demographic equilibrium in the disease-free state [78].

For *Anopheles* mosquitoes with a natural mortality rate of 18 days and baseline population $N_m(0) = 50{,}000$.

Nigeria has an average of 55 million cases of malaria and 90,000 malaria mortality (δ_h) annually. The mortality rate due to malaria is calculated as $\delta_h = \frac{90000}{500000} = 0.0000018$ per day [54].

The total rate leaving the exposed human class is k_3. If the mean exposed duration is $D_E = 11$ days and $p_A = 0.573$ (57.3% go asymptomatic), $p_I = 0.427$ (42.7% become symptomatic), then

$$k_3 = \frac{1}{D_E} = \frac{1}{11} = 0.0909 \text{ day}^{-1},$$

$$\vartheta_h = p_A\, k_3 = 0.573 \times 0.0909 = 0.0520 \text{ day}^{-1},$$

$$\kappa_h = p_I\, k_3 = 0.427 \times 0.0909 = 0.0388 \text{ day}^{-1}.$$

If the average mosquito extrinsic incubation period, $D_{EIP} = 11$ days:

$$\kappa_m = \frac{1}{D_{EIP}} = \frac{1}{11} = 0.0909 \text{ day}^{-1}.$$

assuming that the human and mosquito natural mortality rates, μ_h and μ_m are sufficiently small to be neglected [32, 65, 76]

From the concept of half life, $t_{\frac{1}{2}}$, the rate of loss of immunity for $t_{\frac{1}{2}} = 1$ year is given by $\omega_h = \frac{\ln(2)}{365} \approx 0.00190$ day^{-1} [31].

The average malaria vaccine efficacy can be taken as $\sigma_h = 60.5\%$ [70, 66, 22, 79], $\mu_m = 0.1429$ [47] and $\Lambda_m = 0.7$ [60].

3.2. *Sensitivity Analysis*

The local sensitivity index (SI) for each of the model parameters in system 2.3 is obtained by calculating the normalized forward sensitivity index with respect to a parameter Ψ [4, 10, 12, 18, 75, 35]. Therefore, $\mathcal{R}_e$ is studied in relation to slight variations in parameter values for both positive and negative SI.

Definition 1

In relation to a parameter Ψ, the normalized forward SI of $\mathcal{R}_e$ is defined by

$$S_{\Psi}^{\mathcal{R}_e} = \frac{\partial \mathcal{R}_e}{\partial \Psi} \times \frac{\Psi}{\mathcal{R}_e} \tag{3.3}$$

The SI expression for each of the parameters in $\mathcal{R}_e$ is obtained using equation 3.3. The SI of $\mathcal{R}_e$ with regard to ν_h, for example, is provided as

$$S_{\nu_h}^{\mathcal{R}_e} = \frac{\partial \mathcal{R}_e}{\partial \nu_h} \times \frac{\nu_h}{\mathcal{R}_e} \approx -\frac{11}{100}$$

Consequently, equation 3.3 can be used to get the SI for each parameter of $\mathcal{R}_e$. Therefore, the parameter values in Table 2.1 are used to evaluate the SI of each parameter with respect to $\mathcal{R}_e$.

Table 3.2 reveals that the parameters $\mu_h, \alpha_m, \beta_{hm}, \beta_{mh}, \kappa_m, \xi_h, \kappa_h, \tau_h$, and ϵ have positive sensitivity indices (SI), whereas $\alpha_h, \gamma_h, \nu_h, \mu_m, \sigma_h, \delta_h, \varphi_h$, and ϑ_h have negative values. A positive SI signifies that $\mathcal{R}_e$ varies in the same direction as the parameter, while a negative SI indicates an opposite effect. For instance, $S_{\nu_h}^{\mathcal{R}_e} \approx -0.113$ shows that doubling the vaccine uptake rate would reduce $\mathcal{R}_e$ by about 11.3%, thus lowering the potential for disease spread. In contrast, $S_{\beta_{hm}}^{\mathcal{R}_e} \approx 0.5$ implies that a 100% rise in the mosquito-to-human transmission probability would lead to a 50% increase in $\mathcal{R}_e$. The most influential parameters are μ_m ($S \approx -1.31$), ϵ ($S \approx 1.00$), and the transmission probabilities β_{hm}, β_{mh} ($S \approx 0.5$), underscoring the importance of vector control and

Table 3.1. Baseline parameter values and their sources

Parameter	Value	Source
α_h	0.004215	Estimated
α_m	0.7000	[60]
μ_h	5.04×10^{-5}	Estimated
μ_m	0.1429	Estimated
δ_h	1.8×10^{-6}	Estimated
ω_h	0.00190	Estimated
β_{hm}	0.729255	[7]
β_{mh}	0.837773	[7]
ν_h	$[0, 1]$	Assumed
ϵ	0.49	[53]
ξ_h	0.0015	Assumed
σ_h	0.605	Estimated
ϑ_h	0.0520	Estimated
κ_h	0.0388	Estimated
κ_m	0.0909	Estimated
τ_h	0.05	Assumed
φ_h	0.01	Assumed
γ_h	0.0092	[53]
η	$[0, 1]$	Assumed
ρ_h	0.001	Assumed

Table 3.2. Partial derivatives $\frac{\partial R_e}{\partial \Psi}$ and normalized sensitivity indices $S_{\Psi}^{\mathcal{R}_e}$ for each parameter at baseline

Parameter	$\frac{\partial R_e}{\partial \Psi}$	$S_{\Psi}^{\mathcal{R}_e}$
α_h	-57.08	-0.5000
α_m	$+0.4087$	$+0.5000$
μ_h	$+9.91 \times 10^3$	$+0.5004$
μ_m	-4.254	-1.3056
δ_h	-5.42	-9.73×10^{-5}
ω_h	0	0.0000
β_{hm}	$+0.3426$	$+0.5000$
β_{mh}	$+0.2926$	$+0.5000$
ν_h	-19.50	-0.1129
ϵ	$+0.6826$	$+1.0000$
ξ_h	$+20.00$	$+0.1092$
σ_h	-0.4202	-0.2585
ϑ_h	-0.0206	-0.0225
κ_h	$+0.0215$	$+0.0228$
κ_m	$+1.146$	$+0.3056$
τ_h	$+0.0441$	$+0.0441$
φ_h	-0.0439	-0.0439
γ_h	-27.09	-0.4972
η	0	0.0000
ρ_h	0	0.0000

contact reduction. Therefore, strategies that strengthen vaccine uptake and efficacy (linked to negative SI) and

simultaneously suppress mosquito survival and biting frequency (linked to positive SI) are the most effective in reducing malaria transmission.

The computed values of the partial derivatives $\left(\frac{\partial R_e}{\partial \Psi}\right)$ describe how R_e responds to infinitesimal changes in each parameter. A positive derivative implies that increasing the parameter raises R_e, thereby enhancing malaria transmission, whereas a negative derivative indicates that increasing the parameter reduces R_e and supports disease control.

The relative magnitudes of these derivatives highlight the parameters to which R_e is most responsive. In particular, $\mu_h, \gamma_h, \nu_h, \xi_h,$ and μ_m exhibit the largest absolute derivative values, showing that even small shifts in these parameters can substantially alter transmission potential. By contrast, parameters such as ω_h, η and ρ_h display near-zero derivatives, indicating negligible impact on R_e under the baseline conditions.

When considered alongside the normalized sensitivity indices, these findings emphasize that mosquito mortality μ_m (negative influence), human-to-mosquito and mosquito-to-human transmission probabilities (β_{hm}, β_{mh}), and the contact rate ϵ (positive influence) are the dominant drivers of malaria spread. On the intervention side, vaccine uptake ν_h and efficacy σ_h (both negative influence) represent important levers for reducing R_e. Thus, parameters with both large derivative magnitudes and strong sensitivity indices emerge as priority targets for malaria control, offering a quantitative foundation for guiding interventions and optimizing resource allocation.

4. Formulation of an Optimal Control Problem (OCP)

This section applies optimal control theory to determine the most effective combination of interventions for reducing malaria transmission. In the context of malaria epidemiology, the objective is to minimize the disease burden in both human and mosquito populations, while accounting for the economic and operational costs of implementing the control strategies.

We introduce three time-dependent interventions:

(i) $\psi_1(t) =$ Insecticide-Treated Nets (ITNs);

(ii) $\psi_2(t) =$ Improved Diagnostic Surveillance; and

(iii) $\psi_3(t) =$ Environmental Sanitation.

(i) The control variable $0 \leq \psi_1(t) \leq 1$ represents the use of ITNs, which serve as a personal protection measure against mosquito bites. The use of ITNs reduces the rate at which susceptible humans are bitten by infectious mosquitoes, and simultaneously reduces the likelihood of mosquitoes becoming infected after biting infectious humans. Thus, this intervention decreases the effective contact between humans and mosquitoes. As a result, the forces of infection for both populations are modified as follows: the human force of infection becomes $\lambda_h^c = (1 - \psi_1(t))\lambda_h$, and the mosquito force of infection becomes $\lambda_m^c = (1 - \psi_1(t))\lambda_m$.

(ii) The control variable $0 \leq \psi_2(t) \leq 1$ represents improved diagnostic surveillance and case detection efforts, such as enhanced laboratory testing, rapid diagnostic tools, and active case finding. This intervention increases the rate at which exposed humans are correctly detected and moved into either asymptomatic or symptomatic compartments for appropriate management. As a result, the disease progression parameters are modified to reflect earlier detection. Specifically, the rate of progression from $E_h(t)$ to $I_h(t)$ is adjusted as $\kappa_h^c = \kappa_h + \theta_1\psi_2(t)$, and the rate from asymptomatic to symptomatic becomes $\tau_h^c = \tau_h + \theta_2\psi_2(t)$, where θ_1 and θ_2 are positive constants representing the effectiveness of surveillance.

(iii) The control variable $0 \leq u_3(t) \leq 1$ denotes environmental sanitation efforts aimed at disrupting mosquito breeding habitats. Such interventions may include drainage of stagnant water, proper waste disposal, clearing of bushes, and other vector habitat modification strategies. These efforts reduce the mosquito population by decreasing the recruitment rate of mosquitoes and increasing their mortality rate. Consequently, mosquito recruitment rate is modified as $\alpha_m^c = (1 - u_3(t))\alpha_m$, and the natural mosquito death rate is increased to $\mu_m^c = \mu_m + u_3(t)\mu_m$.

By formulating an objective functional that balances infection prevalence against the costs and feasibility of these interventions, we aim to identify the optimal time-dependent profiles of $\psi_i(t), i = 1, 2, 3$ that achieve the greatest reduction in malaria cases and vector density over the endemic region:

$$J(\psi_1, \psi_2, \psi_3) = \int_0^{t_f} \left[\kappa_1 A_h(t) + \kappa_2 I_h(t) + \kappa_3 I_m(t) + \frac{1}{2} \left(\omega_1 \psi_1^2(t) + \omega_2 \psi_2^2(t) + \omega_3 \psi_3^2(t) \right) \right] dt, \tag{4.1}$$

subject to the non-linear ODEs below:

$$\begin{cases} \frac{dS_h}{dt} = \alpha_h + w_h R_h + \xi_h V_h - \nu_h S_h - \lambda_h^c S_h - \mu_h S_h, \\ \frac{dV_h}{dt} = \nu_h S_h - (1 - \sigma_h)\lambda_h^c V_h - \xi_h V_h - \mu_h V_h, \\ \frac{dE_h}{dt} = \lambda_h^c S_h + (1 - \sigma_h)\lambda_h^c V_h - \vartheta_h E_h - \kappa_h^c E_h - \mu_h E_h, \\ \frac{dA_h}{dt} = \vartheta_h E_h - \tau_h^c A_h - \varphi_h A_h - \mu_h A_h, \\ \frac{dI_h}{dt} = \kappa_h^c E_h + \tau_h^c A_h - \gamma_h I_h - (\delta_h + \mu_h) I_h, \\ \frac{dT_h}{dt} = \eta \gamma_h I_h - \rho_h T_h - (\delta_h + \mu_h) T_h, \\ \frac{dR_h}{dt} = \varphi_h A_h + \gamma_h (1 - \eta) I_h + \rho_h T_h - w_h R_h - \mu_h R_h, \\ \frac{dS_m}{dt} = (1 - \psi_3(t))\alpha_m - \lambda_m^c S_m - (1 + \psi_3(t))\mu_m S_m, \\ \frac{dE_m}{dt} = \lambda_m^c S_m - \kappa_m E_m - (1 + \psi_3(t))\mu_m E_m, \\ \frac{dI_m}{dt} = \kappa_m E_m - (1 + \psi_3(t))\mu_m I_m, \end{cases} \tag{4.2}$$

with the initial conditions given by 2.4. The modified forces of infection are defined as:

$$\lambda_h^c = (1 - \psi_1(t)) \frac{\beta_{hm} \epsilon I_m}{N_h}, \quad \lambda_m^c = (1 - \psi_1(t)) \frac{\beta_{mh} \epsilon I_h}{N_h}$$

. The modified progression rates under improved surveillance are:

$$\kappa_h^c = \kappa_h + \theta_1 \psi_2(t), \quad \tau_h^c = \tau_h + \theta_2 \psi_2(t)$$

where θ_1, θ_2 are positive constants reflecting the strength of the surveillance, t_f stands for the final time for the control strategies implementation. The balancing weight constants, $\kappa_i > 0,\ i = 1, 2, 3$, are for asymptomatic humans, infectious humans and infectious mosquitoes. The terms $\frac{1}{2}\omega_i \psi_i^2(t),\ i = 1, 2, 3$ denote the costs associated with implementing insecticide-treated nets (ITNs), improved diagnostic surveillance, and environmental sanitation, respectively.

We use the idea from [6, 30, 37, 48] to get the best controls in order to minimize the objective functional

$$J(\psi_1^*(t), \psi_2^*(t), \psi_3^*(t)) = \min_{\Phi} J(\psi_1(t), \psi_2(t), \psi_3(t)) \tag{4.3}$$

where $\Phi = \psi_i(t), i = 1, 2, 3$ are lebesque measurable functions with $\psi_i(t) \in [0, 1] : 0 \leq t \leq t_f$ because the state and control variables are non-negative, Φ exists and is bounded, closed, and convex.

The application of optimal control allows for the investigation of optimal intervention strategies in accordance with Pontryagin's Maximum Principle. This principle is employed to reformulate the controlled system equations and the objective functional into a minimization problem involving the pointwise Lagrangian $\mathcal{L}$ with respect to $\psi_1(t)$, $\psi_2(t)$, and $\psi_3(t)$. The aim is to determine the optimal time-dependent control profiles that minimize $\mathcal{L}$. This approach aligns with the standard methodology presented in [9], where the Hamiltonian $\mathcal{H}$ is analyzed to characterize the necessary conditions for optimality and to derive the optimal control strategy. The Hamiltonian is

given as:

$$\begin{aligned}\mathcal{H} &= \kappa_1 A_h + \kappa_2 I_h + \kappa_3 I_m + \frac{1}{2}\left(\omega_1\psi_1^2 + \omega_2\psi_2^2 + \omega_3\psi_3^2\right)\\ &+ \lambda_{S_h}\left(\alpha_h + w_h R_h + \xi_h V_h - \nu_h S_h - \lambda_h^c S_h - \mu_h S_h\right)\\ &+ \lambda_{V_h}\left(\nu_h S_h - (1-\sigma_h)\lambda_h^c V_h - \xi_h V_h - \mu_h V_h\right)\\ &+ \lambda_{E_h}\left(\lambda_h^c S_h + (1-\sigma_h)\lambda_h^c V_h - \vartheta_h E_h - \kappa_h^c E_h - \mu_h E_h\right)\\ &+ \lambda_{A_h}\left(\vartheta_h E_h - \tau_h^c A_h - \varphi_h A_h - \mu_h A_h\right)\\ &+ \lambda_{I_h}\left(\kappa_h^c E_h + \tau_h^c A_h - \gamma_h I_h - (\delta_h + \mu_h) I_h\right)\\ &+ \lambda_{T_h}\left(\eta\gamma_h I_h - \rho_h T_h - (\delta_h + \mu_h) T_h\right)\\ &+ \lambda_{R_h}\left(\varphi_h A_h + \gamma_h(1-\eta) I_h + \rho_h T_h - w_h R_h - \mu_h R_h\right)\\ &+ \lambda_{S_m}\left((1-\psi_3)\alpha_m - \lambda_m^c S_m - (1+\psi_3)\mu_m S_m\right)\\ &+ \lambda_{E_m}\left(\lambda_m^c S_m - \kappa_m E_m - (1+\psi_3)\mu_m E_m\right)\\ &+ \lambda_{I_m}\left(\kappa_m E_m - (1+\psi_3)\mu_m I_m\right).\end{aligned} \tag{4.4}$$

Theorem 6
For the OCP given by (4.1)-(4.2) with the initial conditions at $t = 0$, there exists $(\psi_1^*(t), \psi_2^*(t), \psi_3^*(t)) \in \mathbf{U}$ such that $J(\psi_1^*(t), \psi_2^*(t), \psi_3^*(t)) = \min_{\psi_1(t),\psi_2(t),\psi_3(t)\in\mathbf{U}} J(\psi_1(t), \psi_2(t), \psi_3(t))$.

Proof
The results in Theorem 6 are established by adopting the techniques in [9, 14, 15, 28]. Thus, the following characteristics will be established:

i The control set $\mathbf{U}$ associated with each state variable equation is non-empty, convex and closed.

ii Non-negative solutions of the system 4.2 exists and it is bounded.

iii The boundedness of each right-hand side expression in model 2.3 is a linear function of $\mathbf{U}$, which varies with time and depends on the state variables.

iv The integrand in the objective function 4.1, expressed as

$$\kappa_1 A_h(t) + \kappa_2 I_h(t) + \kappa_3 I_m(t) + \frac{1}{2}\left(\omega_1\psi_1^2(t) + \omega_2\psi_2^2(t) + \omega_3\psi_3^2(t)\right)$$

convex in $\mathbf{U}$.

i The control set $\mathbf{U}$ is non-empty and closed since it contains all of its limit points. Therefore, given $\lambda \in [0, 1]$ and any two arbitrary points $x, y \in \mathbf{U}$, where $\mathbf{x} = (\mathbf{x_1}, \mathbf{x_2}, \mathbf{x_3})$ and $\mathbf{y} = (\mathbf{y_1}, \mathbf{y_2}, \mathbf{y_3})$, then $\lambda\mathbf{x_i} + (1-\lambda)\mathbf{y_i} \in \mathbf{U}$ for $i = 1, 2, 3$ satisfying the convexity property of the control set.

ii We take into consideration the objective function $J(\psi_1(t), \psi_2(t), \psi_3(t))$ since the state and control variables in system 4.2 are positive and the control set $\mathbf{U}$ is closed and convex, as demonstrated above. Finding the ideal control is made easier by the convexity that means every local minimum is also a global minimum as the integrand of J is a convex function of the control variables $\psi_1(t), \psi_2(t), \psi_3(t)$ on the control set $\mathbf{U}$. Additionally, for any admissible control $\psi_i(t) = (\psi_1(t), \psi_2(t), \psi_3(t))$, there exist positive constants χ_1, χ_2 and $\epsilon > 1$, such that

$$\begin{aligned} J =& \kappa_1 A_h(t) + \kappa_2 I_h(t) + \kappa_3 I_m(t) + \frac{1}{2}\left(\omega_1\psi_1^2(t) + \omega_2\psi_2^2(t) + \omega_3\psi_3^2(t)\right) \\ &\geq \omega_1\psi_1^2(t) + \omega_2\psi_2^2(t) + \omega_3\psi_3^2(t) \\ &\geq \omega_1\psi_1^2(t) + \omega_2\psi_2^2(t) + \omega_3\psi_3^2(t) - \chi_2 \qquad \text{Since } \omega_1\psi - \omega_1 \leq 0 \\ &\geq \min\left(\frac{1}{2}\omega_1 + \frac{1}{2}\omega_2 + \frac{1}{2}\omega_3\right)(\psi_1^2(t) + \omega_2\psi_2^2(t) + \omega_3\psi_3^2(t)) - \omega_1 \\ &\geq \chi_1\|u\|^2, \end{aligned} \tag{4.5}$$

where $\chi_2 = \min\left(\frac{1}{2}\omega_1 + \frac{1}{2}\omega_2 + \frac{1}{2}\omega_3\right)$, $\chi_1\omega_1$ and $\epsilon = 2$.

It is noted that the inequality guarantees that J is convex with regard to the control variables. An optimal control is implied by the convexity of J, the boundedness of the state variables, and both of these factors. Lastly, using the Direct Method in the Calculus of Variations, we determine that the closed and convex control set $\mathbf{U}$ contains the optimal controls $\psi_i(t)$ that minimize the objective function J. As a result, it is established that 4.1 subject to system of equations 4.2 has an optimal control.

iii We use the method described in [9] to prove this condition. Let

$$\mathcal{H}(X, \psi, \mu) = H(X, \psi) + G(\mu)X$$

$$\text{where} \quad G(\mu) = \begin{bmatrix} -\mu & 0 & 0 & 0 & 0 & 0 & 0 & 0 & 0 & 0 \\ 0 & -\mu & 0 & 0 & 0 & 0 & 0 & 0 & 0 & 0 \\ 0 & 0 & -\mu & 0 & 0 & 0 & 0 & 0 & 0 & 0 \\ 0 & 0 & 0 & -\mu & 0 & 0 & 0 & 0 & 0 & 0 \\ 0 & 0 & 0 & 0 & -\mu & 0 & 0 & 0 & 0 & 0 \\ 0 & 0 & 0 & 0 & 0 & -\mu & 0 & 0 & 0 & 0 \\ 0 & 0 & 0 & 0 & 0 & 0 & -\mu & 0 & 0 & 0 \\ 0 & 0 & 0 & 0 & 0 & 0 & 0 & -\mu & 0 & 0 \\ 0 & 0 & 0 & 0 & 0 & 0 & 0 & 0 & -\mu & 0 \\ 0 & 0 & 0 & 0 & 0 & 0 & 0 & 0 & 0 & -\mu \end{bmatrix}, \quad X = \begin{bmatrix} S_h(t) \\ V_h(t) \\ E_h(t) \\ A_h(t) \\ I_h(t) \\ T_h(t) \\ R_h(t) \\ S_m(t) \\ E_m(t) \\ I_m(t) \end{bmatrix},$$

$$H(X, \psi, \mu) = \begin{bmatrix} \alpha_h + w_h R_h + \xi_h V_h - \nu_h S_h - \lambda_h^c S_h \\ \nu_h S_h - (1-\sigma_h)\lambda_h^c V_h - \xi_h V_h \\ \lambda_h^c S_h + (1-\sigma_h)\lambda_h^c V_h - \vartheta_h E_h - \kappa_h^c E_h \\ \vartheta_h E_h - \tau_h^c A_h - \varphi_h A_h \\ \kappa_h^c E_h + \tau_h^c A_h - \gamma_h I_h - \mu_h I_h \\ \eta\gamma_h I_h - \rho_h T_h - \mu_h T_h \\ \varphi_h A_h + \gamma_h(1-\eta) I_h + \rho_h T_h - w_h R_h \\ (1-\psi_3(t))\alpha_m - \lambda_m^c S_m - \psi_3(t)\mu_m S_m \\ \lambda_m^c S_m - \kappa_m E_m - \psi_3(t)\mu_m E_m \\ \kappa_m E_m - \psi_3(t)\mu_m I_m \end{bmatrix} \tag{4.6}$$

Given the initial conditions 2.4, a non-negative bounded OCP and Lebesgue measurable controls exist. The OCP provided by model (4.2) can be expressed as follows:

$$\frac{d\mathbf{X}}{dt} = \mathbf{D}(\psi_{\mathbf{i}}(\mathbf{t}))\mathbf{X} + \mathbf{G}(\psi_{\mathbf{i}}(\mathbf{t}), \mathbf{X}) \tag{4.7}$$

Equation 4.7 has bounded coefficients and is a non-linear coupled system. Let

$$\mathbf{H}(\mathbf{X}) = \mathbf{D}\mathbf{X} + \mathbf{G}(\psi_{\mathbf{i}}(\mathbf{t}), \mathbf{X}) \tag{4.8}$$

Therefore, the first equation of (4.2) shows that

$$\begin{aligned}|\mathbf{G}(\psi_{\mathbf{i}}(\mathbf{t}),\mathbf{X_1})-\mathbf{G}(\psi_{\mathbf{i}}(\mathbf{t}),\mathbf{X_2})| \leq & c_1\,|S_{h1}-S_{h2}|+c_2\,|V_{h1}-V_{h2}|+c_3\,|E_{h1}-E_{h2}|+c_4\,|A_{h1}-A_{h2}|\\ &+c_5\,|I_{h1}-I_{h2}|+c_6\,|T_{h1}-T_{h2}|+c_7\,|R_{h1}-R_{h2}|+c_8\,|S_{m1}-S_{m2}|\\ &+c_9\,|E_{m1}-E_{m2}|+c_{10}\,|I_{m1}-I_{hm2}|\\ \leq & c\big(\,|S_{h1}-S_{h2}|+|V_{h1}-V_{h2}|+|E_{h1}-E_{h2}|+|A_{h1}-A_{h2}|\\ &+|I_{h1}-I_{h2}|+|T_{h1}-T_{h2}|+|R_{h1}-R_{h2}|+|S_{m1}-S_{m2}|\\ &+|E_{m1}-E_{m2}|+|I_{m1}-I_{hm2}|\,\big)\end{aligned} \tag{4.9}$$

where $X_1=\big(S_{h1},V_{h1},E_{h1},A_{h1},I_{h1},T_{h1},R_{h1},S_{m1},E_{m1},I_{m1}\big)$, and $X_2=\big(S_{h2},V_{h2},E_{h2},A_{h2},I_{h2},T_{h2},R_{h2},S_{m2},E_{m2},I_{m2}\big)$ and $c=max\big(c_i,i=1,2,\ldots,10\big)$. It is noted that c is independent of the state variables. Hence, the following inequality holds:

$$|H(X_1)-H(X_2)|\leq c\,|X_1-X_2| \tag{4.10}$$

for $c=\sum_{i=1}^{10}a_1+\|H\|^2\leq\infty$. Thus, $H(X)$ is Lipschitz continuous. Given the control variables $\psi_i,i=1,2,3$ and the initial conditions 2.4, it follows that solutions of the control model 4.2 exist.

iv Let $\boldsymbol{\psi}(t)=(\psi_1(t),\psi_2(t),\psi_3(t))^\top$ and define, for fixed t,

$$f(\boldsymbol{\psi}) \;=\; \kappa_1A_h(t)+\kappa_2I_h(t)+\kappa_3I_m(t) \;+\; \tfrac{1}{2}\big(\omega_1\psi_1^2+\omega_2\psi_2^2+\omega_3\psi_3^2\big).$$

The terms $\kappa_1A_h(t)+\kappa_2I_h(t)+\kappa_3I_m(t)$ are constant with respect to $\boldsymbol{\psi}$ (for fixed t), so convexity in $\boldsymbol{\psi}$ is determined by the quadratic term.

Compute the gradient and Hessian with respect to $\boldsymbol{\psi}$:

$$\nabla_{\boldsymbol{\psi}}f(\boldsymbol{\psi})=\begin{pmatrix}\omega_1\psi_1\\ \omega_2\psi_2\\ \omega_3\psi_3\end{pmatrix},\qquad \nabla^2_{\boldsymbol{\psi}}f(\boldsymbol{\psi})=\begin{pmatrix}\omega_1&0&0\\0&\omega_2&0\\0&0&\omega_3\end{pmatrix}.$$

For any $v=(v_1,v_2,v_3)^\top$,

$$v^\top\nabla^2_{\boldsymbol{\psi}}f(\boldsymbol{\psi})\,v=\omega_1v_1^2+\omega_2v_2^2+\omega_3v_3^2.$$

Hence, if $\omega_i\geq0$ for $i=1,2,3$, the Hessian is positive semidefinite and f is convex in $\boldsymbol{\psi}$. If $\omega_i>0$ for all i the Hessian is positive definite and f is strictly convex.

Since the objective functional is

$$J(\psi_1,\psi_2,\psi_3)=\int_0^{t_f}f\big(\boldsymbol{\psi}(t)\big)\,dt,$$

and the pointwise integrand $f(\boldsymbol{\psi}(t))$ is convex in $\boldsymbol{\psi}(t)$ for each t, the functional J is convex in the control functions $\boldsymbol{\psi}(\cdot)$ on any convex admissible control set (for example measurable controls taking values in a convex set like $[0,1]^3$). Moreover J is strictly convex if $\omega_i>0$ for all i.

□

4.1. The Uniqueness of the Optimal Control

The optimality system that follows is obtained by using the method in [9, 35, 37]. Pontryagin's Maximum Principle is used to determine the uniqueness of the optimal control of the malaria epidemiological model. This principle establishes the prerequisites for optimality, and if it results in a singular solution, it validates that the optimal

control is unique. Here, the goal is to minimize the cost functional in equation (4.1) while taking into account the dynamics of malaria transmission as given by system (2.3), which ensures the existence of an optimal control. If $(X(t), \mathbf{U}(t))$ is an optimal pair for the control problem, then there exists a non-trivial vector function, based on Pontryagin's Maximum Principle.

$$\boldsymbol{\lambda}(t) = (\lambda_{S_h}, \lambda_{V_h}, \lambda_{E_h}, \lambda_{A_h}, \lambda_{I_h}, \lambda_{T_h}, \lambda_{R_h}, \lambda_{S_m}, \lambda_{E_m}, \lambda_{I_m})^\top$$

.

The adjoint variables satisfy

$$\frac{d\lambda_i}{dt} = -\frac{\partial \mathcal{H}}{\partial x_i}, \quad \lambda_i(t_f) = 0, \quad i = 1, 2, \ldots, 10,$$

where x_i represents the ith component of the state vector $X(t)$. The optimality condition

$$\frac{\partial \mathcal{H}}{\partial \psi_j} = 0, \quad j = 1, 2, 3,$$

yields the explicit control characterizations

$$\psi_j^*(t) = \min\left\{\max\left\{0, -\frac{1}{\omega_j}\frac{\partial\left(\boldsymbol{\lambda}^\top F(X, \mathbf{U})\right)}{\partial \psi_j}\right\}, 1\right\}, \quad j = 1, 2, 3.$$

These necessary conditions, together with the convexity of the integrand in $\mathbf{U}$, guaranteed the uniqueness of the optimal control for the malaria model.

Theorem 7
Given the optimal control $\psi_1^*(t), \psi_2^*(t), \psi_3^*(t)$ and solutions of the state variables $\lambda_{S_h}^*, \lambda_{V_h}^*, \lambda_{E_h}^*, \lambda_{A_h}^*, \lambda_{I_h}^*, \lambda_{T_h}^*, \lambda_{R_h}^*, \lambda_{S_m}^*, \lambda_{E_m}^*, \lambda_{I_m}^*$, then there exists adjoint variables λ_i for $i = (\lambda_{S_h}, \lambda_{V_h}, \lambda_{E_h}, \lambda_{A_h}, \lambda_{I_h}, \lambda_{T_h}, \lambda_{R_h}, \lambda_{S_m}, \lambda_{E_m}, \lambda_{I_m})$ that minimizes $J(\psi_1^*(t), \psi_2^*(t), \psi_3^*(t)$ over Φ satisfying:

$$\begin{aligned}
\dot{\lambda}_{S_h} &= \lambda_{S_h}\left(\nu_h + (1-\psi_1)\frac{\beta_{hm}\epsilon I_m}{N_h} + \mu_h\right) - \lambda_{V_h}\,\nu_h - \lambda_{E_h}\,(1-\psi_1)\frac{\beta_{hm}\epsilon I_m}{N_h},\\
\dot{\lambda}_{V_h} &= -\lambda_{S_h}\,\xi_h + \lambda_{V_h}\left((1-\sigma_h)(1-\psi_1)\frac{\beta_{hm}\epsilon I_m}{N_h} + \xi_h + \mu_h\right) - \lambda_{E_h}\,(1-\sigma_h)(1-\psi_1)\frac{\beta_{hm}\epsilon I_m}{N_h},\\
\dot{\lambda}_{E_h} &= \lambda_{E_h}\left(\vartheta_h + \kappa_h + \theta_1\psi_2 + \mu_h\right) - \lambda_{A_h}\,\vartheta_h - \lambda_{I_h}\,(\kappa_h + \theta_1\psi_2),\\
\dot{\lambda}_{A_h} &= -\kappa_1 + \lambda_{A_h}\left(\tau_h + \theta_2\psi_2 + \varphi_h + \mu_h\right) - \lambda_{I_h}\,(\tau_h + \theta_2\psi_2) - \lambda_{R_h}\,\varphi_h,\\
\dot{\lambda}_{I_h} &= -\kappa_2 + \lambda_{I_h}\left(\gamma_h + \delta_h + \mu_h\right) - \lambda_{T_h}\,\eta\gamma_h - \lambda_{R_h}\,\gamma_h(1-\eta) + (1-\psi_1)\frac{\beta_{mh}\epsilon S_m}{N_h}\,(\lambda_{S_m} - \lambda_{E_m}),\\
\dot{\lambda}_{T_h} &= \lambda_{T_h}\left(\rho_h + \delta_h + \mu_h\right) - \lambda_{R_h}\,\rho_h,\\
\dot{\lambda}_{R_h} &= -\lambda_{S_h}\,w_h + \lambda_{R_h}\left(w_h + \mu_h\right),\\
\dot{\lambda}_{S_m} &= \lambda_{S_m}\left((1-\psi_1)\frac{\beta_{mh}\epsilon I_h}{N_h} + (1+\psi_3)\mu_m\right) - \lambda_{E_m}\,(1-\psi_1)\frac{\beta_{mh}\epsilon I_h}{N_h},\\
\dot{\lambda}_{E_m} &= \lambda_{E_m}\left(\kappa_m + (1+\psi_3)\mu_m\right) - \lambda_{I_m}\,\kappa_m,\\
\dot{\lambda}_{I_m} &= -\kappa_3 + \frac{(1-\psi_1)\beta_{hm}\epsilon}{N_h}\left(\lambda_{S_h}S_h + (1-\sigma_h)\lambda_{V_h}V_h - \lambda_{E_h}\left(S_h + (1-\sigma_h)V_h\right)\right) + \lambda_{I_m}\,(1+\psi_3)\mu_m.
\end{aligned} \tag{4.11}$$

with the control variables $\psi_1^*(t), \psi_2^*(t), \psi_3^*(t)$ and the transversality conditions

$$\lambda_i(t_f) = 0,\ i = (\lambda_{S_h}, \lambda_{V_h}, \lambda_{E_h}, \lambda_{A_h}, \lambda_{I_h}, \lambda_{T_h}, \lambda_{R_h}, \lambda_{S_m}, \lambda_{E_m}, \lambda_{I_m}). \tag{4.12}$$

The following optimality conditions are used to characterize the control variables:

$$\begin{aligned}
\psi_1^* &= \max\Bigg(0, \min\Bigg(1, \frac{1}{\omega_1}\Bigg[(\lambda_{E_h} - \lambda_{S_h})\frac{\beta_{hm}\epsilon I_m}{N_h}S_h + (\lambda_{E_h} - \lambda_{V_h})\frac{\beta_{hm}\epsilon I_m}{N_h}V_h(1-\sigma_h) \\
&\quad + (\lambda_{E_m} - \lambda_{S_m})\frac{\beta_{mh}\epsilon I_h}{N_h}S_m\Bigg]\Bigg)\Bigg), \\
\psi_2^* &= \max\Bigg(0, \min\Bigg(1, \frac{1}{\omega_2}\Bigg[(\lambda_{I_h} - \lambda_{E_h})\theta_1 E_h + (\lambda_{I_h} - \lambda_{A_h})\theta_2 A_h\Bigg]\Bigg)\Bigg), \\
\psi_3^* &= \max\Bigg(0, \min\Bigg(1, \frac{1}{\omega_3}\Bigg[\lambda_{S_m}(\alpha_m + \mu_m S_m) + \lambda_{E_m}\mu_m E_m + \lambda_{I_m}\mu_m I_m\Bigg]\Bigg)\Bigg).
\end{aligned} \tag{4.13}$$

Proof
The Hamiltonian associated with the malaria OCP is defined by

$$\begin{aligned}
\mathcal{H} &= \kappa_1 A_h + \kappa_2 I_h + \kappa_3 I_m + \tfrac{1}{2}\big(\omega_1\psi_1^2 + \omega_2\psi_2^2 + \omega_3\psi_3^2\big) \\
&\quad + \lambda_{S_h}\Big(\alpha_h + w_h R_h + \xi_h V_h - \nu_h S_h - (1-\psi_1)\frac{\beta_{hm}\epsilon I_m}{N_h}S_h - \mu_h S_h\Big) \\
&\quad + \lambda_{V_h}\Big(\nu_h S_h - (1-\sigma_h)(1-\psi_1)\frac{\beta_{hm}\epsilon I_m}{N_h}V_h - \xi_h V_h - \mu_h V_h\Big) \\
&\quad + \lambda_{E_h}\Big((1-\psi_1)\frac{\beta_{hm}\epsilon I_m}{N_h}S_h + (1-\sigma_h)(1-\psi_1)\frac{\beta_{hm}\epsilon I_m}{N_h}V_h \\
&\quad - \vartheta_h E_h - (\kappa_h + \theta_1\psi_2)E_h - \mu_h E_h\Big) \\
&\quad + \lambda_{A_h}\Big(\vartheta_h E_h - (\tau_h + \theta_2\psi_2)A_h - \varphi_h A_h - \mu_h A_h\Big) \\
&\quad + \lambda_{I_h}\Big((\kappa_h + \theta_1\psi_2)E_h + (\tau_h + \theta_2\psi_2)A_h - \gamma_h I_h - (\delta_h + \mu_h)I_h\Big) \\
&\quad + \lambda_{T_h}\Big(\eta\gamma_h I_h - \rho_h T_h - (\delta_h + \mu_h)T_h\Big) \\
&\quad + \lambda_{R_h}\Big(\varphi_h A_h + \gamma_h(1-\eta)I_h + \rho_h T_h - w_h R_h - \mu_h R_h\Big) \\
&\quad + \lambda_{S_m}\Big((1-\psi_3)\alpha_m - (1-\psi_1)\frac{\beta_{mh}\epsilon I_h}{N_h}S_m - (1+\psi_3)\mu_m S_m\Big) \\
&\quad + \lambda_{E_m}\Big((1-\psi_1)\frac{\beta_{mh}\epsilon I_h}{N_h}S_m - \kappa_m E_m - (1+\psi_3)\mu_m E_m\Big) \\
&\quad + \lambda_{I_m}\Big(\kappa_m E_m - (1+\psi_3)\mu_m I_m\Big).
\end{aligned} \tag{4.14}$$

The partial derivatives of the Hamiltonian function, **H**, with respect to each of the model's state variables are taken to obtain the adjoint system:

$$\dot{\lambda}_{S_h} = -\frac{\partial\mathcal{H}}{\partial S_h}, \quad \lambda_{S_h}(t_f) = 0,$$

$$\dot{\lambda}_{V_h} = -\frac{\partial \mathcal{H}}{\partial V_h}, \quad \lambda_{V_h}(t_f) = 0,$$
$$\dot{\lambda}_{E_h} = -\frac{\partial \mathcal{H}}{\partial E_h}, \quad \lambda_{E_h}(t_f) = 0,$$
$$\dot{\lambda}_{A_h} = -\frac{\partial \mathcal{H}}{\partial A_h}, \quad \lambda_{A_h}(t_f) = 0,$$
$$\dot{\lambda}_{I_h} = -\frac{\partial \mathcal{H}}{\partial I_h}, \quad \lambda_{I_h}(t_f) = 0,$$
$$\dot{\lambda}_{T_h} = -\frac{\partial \mathcal{H}}{\partial T_h}, \quad \lambda_{T_h}(t_f) = 0,$$
$$\dot{\lambda}_{R_h} = -\frac{\partial \mathcal{H}}{\partial R_h}, \quad \lambda_{R_h}(t_f) = 0,$$
$$\dot{\lambda}_{S_m} = -\frac{\partial \mathcal{H}}{\partial S_m}, \quad \lambda_{S_m}(t_f) = 0,$$
$$\dot{\lambda}_{E_m} = -\frac{\partial \mathcal{H}}{\partial E_m}, \quad \lambda_{E_m}(t_f) = 0,$$
$$\dot{\lambda}_{I_m} = -\frac{\partial \mathcal{H}}{\partial I_m}, \quad \lambda_{I_m}(t_f) = 0.$$

□

If (x, ψ) is the optimal solution based on the optimality conditions, then $\frac{\partial \mathbf{H}}{\partial \psi_1} = \frac{\partial \mathbf{H}}{\partial \psi_2} = \frac{\partial \mathbf{H}}{\partial \psi_3} = 0$ at $\psi_i = \psi_i^*$

$$\begin{aligned}
\psi_1^* &= \max\left(0, \min\left(1, \frac{1}{\omega_1}\left[(\lambda_{E_h} - \lambda_{S_h})\frac{\beta_{hm}\epsilon I_m}{N_h} S_h + (\lambda_{E_h} - \lambda_{V_h})\frac{\beta_{hm}\epsilon I_m}{N_h} V_h(1-\sigma_h)\right.\right.\right. \\
&\quad \left.\left.\left. + (\lambda_{E_m} - \lambda_{S_m})\frac{\beta_{mh}\epsilon I_h}{N_h} S_m\right]\right)\right), \\
\psi_2^* &= \max\left(0, \min\left(1, \frac{1}{\omega_2}\left[(\lambda_{I_h} - \lambda_{E_h})\theta_1 E_h + (\lambda_{I_h} - \lambda_{A_h})\theta_2 A_h\right]\right)\right), \\
\psi_3^* &= \max\left(0, \min\left(1, \frac{1}{\omega_3}\left[\lambda_{S_m}(\alpha_m + \mu_m S_m) + \lambda_{E_m}\mu_m E_m + \lambda_{I_m}\mu_m I_m\right]\right)\right).
\end{aligned} \tag{4.15}$$

$$\begin{aligned}
\frac{\partial \mathbf{H}}{\partial \psi_1} &= \omega_1\psi_1 - \left((\lambda_{E_h} - \lambda_{S_h})\frac{\beta_{hm}\epsilon I_m}{N_h} S_h + (\lambda_{E_h} - \lambda_{V_h})\frac{\beta_{hm}\epsilon I_m}{N_h} V_h(1-\sigma_h) + (\lambda_{E_m} - \lambda_{S_m})\frac{\beta_{mh}\epsilon I_h}{N_h} S_m\right), \\
\frac{\partial \mathbf{H}}{\partial \psi_2} &= \omega_2\psi_2 - \left((\lambda_{I_h} - \lambda_{E_h})\theta_1 E_h + (\lambda_{I_h} - \lambda_{A_h})\theta_2 A_h\right), \\
\frac{\partial \mathbf{H}}{\partial \psi_3} &= \omega_3\psi_3 - \left(\lambda_{S_m}(\alpha_m + \mu_m S_m) + \lambda_{E_m}\mu_m E_m + \lambda_{I_m}\mu_m I_m\right).
\end{aligned}$$

Hence, the OC functions are given as

$$\begin{cases}
\psi_1^* = \frac{1}{\omega_1}\left((\lambda_{E_h} - \lambda_{S_h})\frac{\beta_{hm}\epsilon I_m}{N_h} S_h + (\lambda_{E_h} - \lambda_{V_h})\frac{\beta_{hm}\epsilon I_m}{N_h} V_h(1-\sigma_h) + (\lambda_{E_m} - \lambda_{S_m})\frac{\beta_{mh}\epsilon I_h}{N_h} S_m\right) \\
\psi_2^* = \frac{1}{\omega_2}\left((\lambda_{I_h} - \lambda_{E_h})\theta_1 E_h + (\lambda_{I_h} - \lambda_{A_h})\theta_2 A_h\right) \\
\psi_3^* = \frac{1}{\omega_3}\left(\lambda_{S_m}(\alpha_m + \mu_m S_m) + \lambda_{E_m}\mu_m E_m + \lambda_{I_m}\mu_m I_m\right)
\end{cases} \tag{4.16}$$

By using the bounds on ψ_i^* and the notion of standard control, we get

$$\psi_i^* = \begin{cases} 0 \; if \; \vartheta_i^* \leq 0 \\ \vartheta_i^* \; if \; 0 < \vartheta_i^* < 1 \\ 1 \; if \; \vartheta_i^* \geq 0 \end{cases}$$

where $i = 1, 2, 3$ and

$$\vartheta_1 = \frac{1}{\omega_1}\left((\lambda_{E_h} - \lambda_{S_h})\frac{\beta_{hm}\epsilon I_m}{N_h}S_h + (\lambda_{E_h} - \lambda_{V_h})\frac{\beta_{hm}\epsilon I_m}{N_h}V_h(1-\sigma_h) + (\lambda_{E_m} - \lambda_{S_m})\frac{\beta_{mh}\epsilon I_h}{N_h}S_m\right)$$

Therefore, ψ_1, the control for ITNs, can be expressed in compact form as

$$\psi_1^*(t) = min\left\{1, max\left\{0, \vartheta_1\right\}\right\}$$

Similarly,

$$\vartheta_2 = \frac{1}{\omega_2}\left((\lambda_{I_h} - \lambda_{E_h})\theta_1 E_h + (\lambda_{I_h} - \lambda_{A_h})\theta_2 A_h\right)$$

Consequently, ψ_2, the control for Improved Diagnostic Surveillance, can be expressed in compact form as

$$\psi_2^*(t) = min\left\{1, max\left\{0, \vartheta_1\right\}\right\}$$

Lastly,

$$\vartheta_3 = \frac{1}{\omega_3}\left(\lambda_{S_m}(\alpha_m + \mu_m S_m) + \lambda_{E_m}\mu_m E_m + \lambda_{I_m}\mu_m I_m\right)$$

Community-based sanitation measures targeting the disruption of mosquito breeding habitats, ψ_3, implies that

$$\psi_3^*(t) = min\left\{1, max\left\{0, \vartheta_3\right\}\right\}$$

5. Results and Discussion

In this section, we analyze the dynamic properties of the malaria model 2.3. The resulting two-point boundary value problem (BVP), corresponding to a sixteen-dimensional optimality system, is solved numerically.

5.1. Autonomous System

We analyze the dynamics of the malaria model using the parameter values presented in Table 3.1. Based on these values, $\mathcal{R}_e$ of system 2.3 is estimated to be approximately $\mathbb{R}_e = 1.2268$.

5.2. Effects of vaccination rate (ν_h) on the Human Population

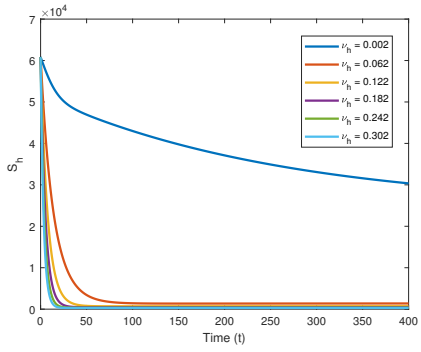

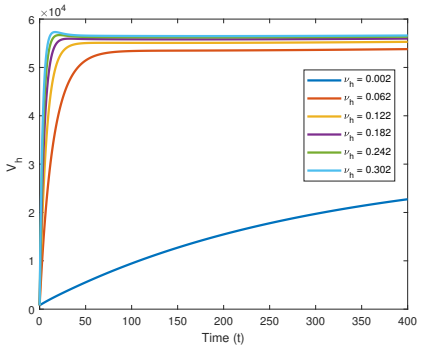

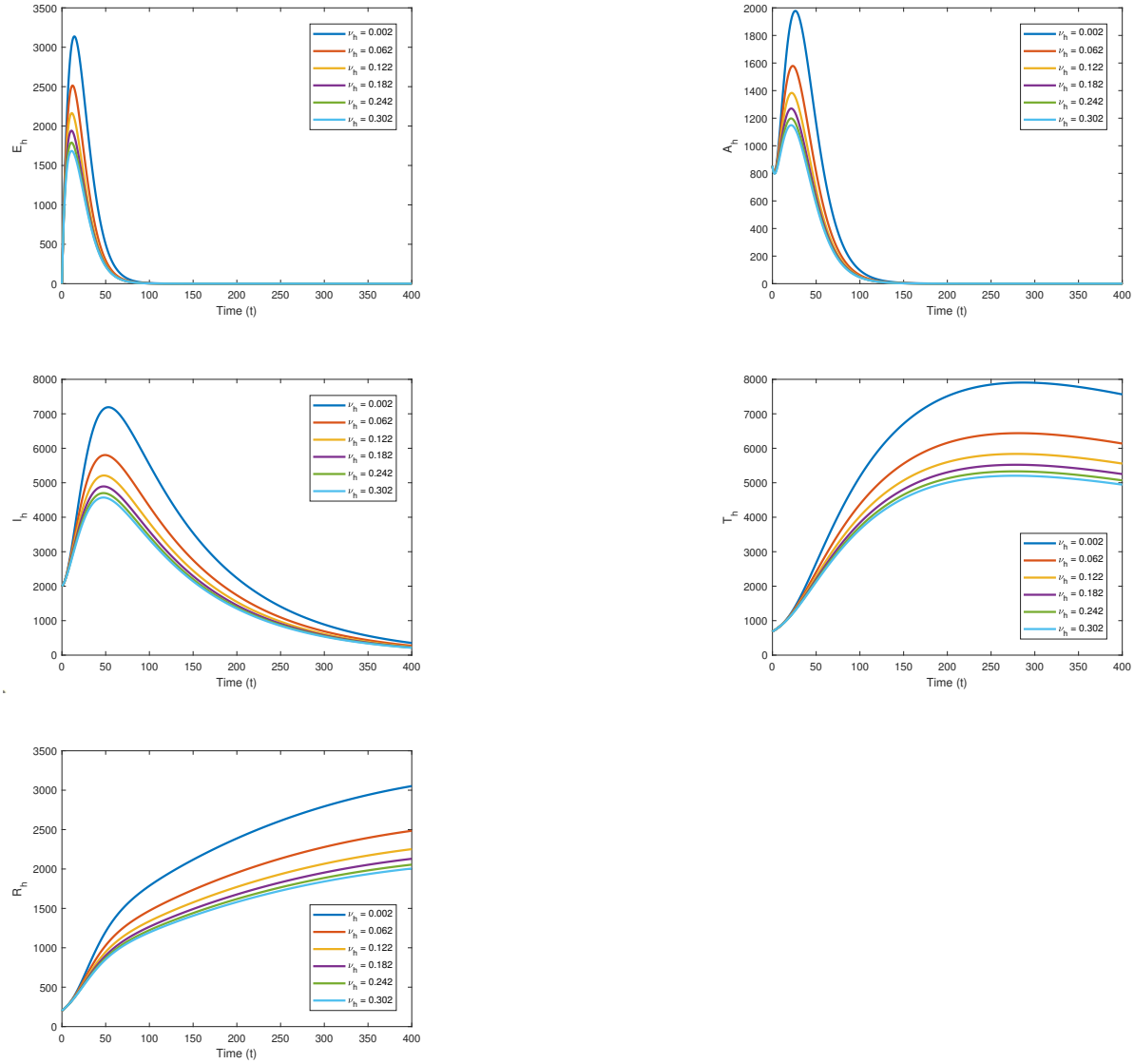

Figures 5.2 - 5.2 reveal the effects of increasing ν_h on each of the classes of the human subpopulation. The population of the susceptible class decreases as u_h increases, as seen in Figure 5.2. This shows that effective malaria vaccines will reduce human susceptability to malaria. Figure 5.2 depicts a significant increase in the vaccinated class. On the other hand, Figures 5.2 - 5.2 reveal that an increase in ν_h causes the population of $E(t)$, $A(t)$, $I(t)$, $T(t)$, and $R(t)$ compartments to decline. This demonstrates how well immunizations work to stop the spread of malaria.

5.3. Correlation of ν_h, σ_h, ϵ and ξ_h with the steady-state vaccinated population (V_h^*)

Figure 5.1a reveals an exceptionally strong positive correlation ($r \approx 0.997$) between the vaccination rate (ν_h) and the resulting steady-state vaccinated population size (V_h^*). This confirms the fundamental principle that increasing the speed of vaccination directly and effectively increases the size of the protected cohort. While the relationship is overwhelmingly positive, it follows a subtle concave-down quadratic trend rather than a purely linear one. This indicates the presence of saturating dynamics within the model. The most substantial absolute gains in V_h^* are achieved at intermediate vaccination rates (e.g., between $\nu_h = 0.4$ and $\nu_h = 0.7$). The slight diminishment in the

rate of increase at the highest values of ν_h is likely due to the increasing competition between the vaccination process and the natural depletion of the susceptible pool from other factors like natural mortality and the vaccine waning rate (ξ_h). The simulation results, represented by blue points, show the model's output across the parameter sweep. The mean steady-state vaccinated population across all simulated rates is approximately 17,500 individuals, with values ranging from around 1,800 to over 33,000. For health policymakers, this analysis underscores that higher vaccination rates are unequivocally beneficial for achieving population-level immunity. The model suggests that while returns may become marginally less pronounced at the highest levels, a strategy focused on maximizing ν_h remains the most effective way to maximize V_h^*. This supports the allocation of resources towards initiatives that accelerate vaccine rollout, such as increasing clinic availability and public outreach campaigns.

Figure 5.1b presents the result of the correlation between the steady-state vaccinated population (V_h^*) and vaccine efficacy (σ_h). The observed strong positive correlation ($r \approx 0.997$) is notable and reveals a non-linear, concave-down quadratic relationship. Contrary to an initial assumption that efficacy primarily protects individuals from infection, the model indicates that higher vaccine efficacy has a secondary, population-level effect: it sustains the size of the vaccinated pool. This occurs because a more efficacious vaccine ($\sigma_h \to 1$) significantly reduces the rate of breakthrough infections, which is a pathway out of the V_h compartment. Consequently, individuals remain vaccinated for longer periods before waning immunity (ξ_h) or natural mortality (μ_h) moves them out. This retention effect allows the constant inflow of new vaccinated individuals (at rate $\nu_h S_h$) to accumulate, resulting in a larger steady-state population V_h^*. The supra-linear increase at very high efficacy levels (e.g., $\sigma_h > 0.95$) suggests a critical threshold beyond which improvements in vaccine quality yield disproportionately large benefits for maintaining population immunity. This implies that investing in the development of high-efficacy vaccines is not only beneficial for individual protection but is also a powerful strategy for achieving and sustaining higher overall vaccination coverage, as it optimizes the durability of the vaccinated state.

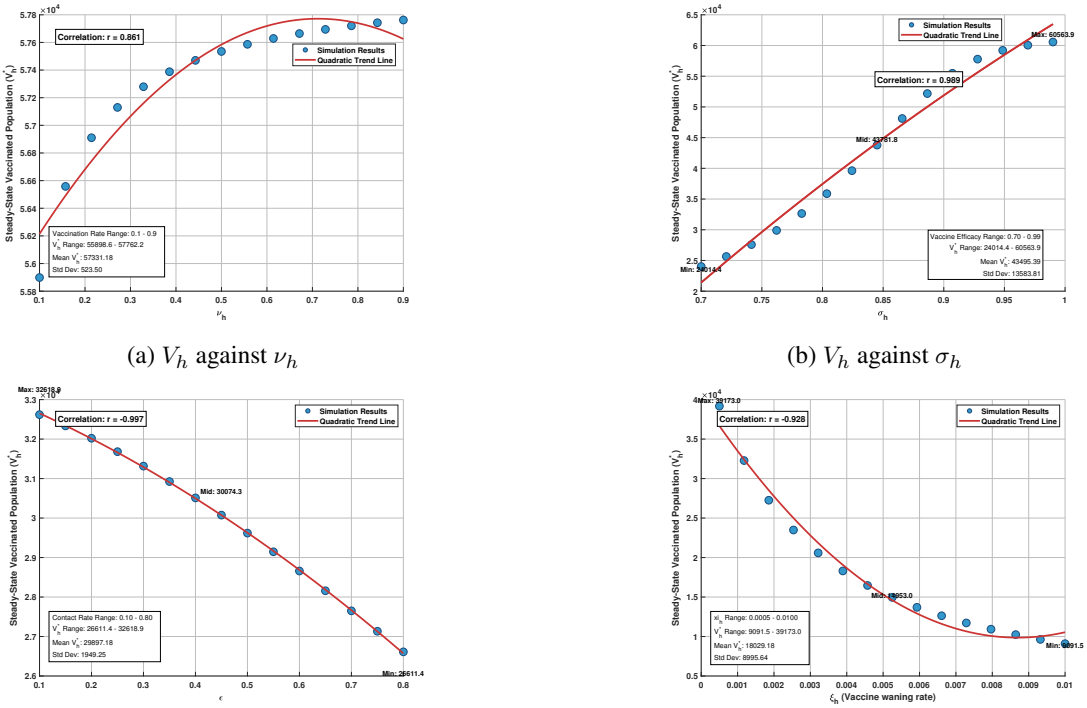

(a) V_h against ν_h

(b) V_h against σ_h

(c) V_h against ϵ

(d) V_h against ξ_h

Figure 5.1. Correlation of ξ_h, ϵ, ν_h and σ_h with V_h^*

Figure 5.1c illustrates a pronounced and robust negative correlation ($r \approx -0.986$) between the human-mosquito contact rate (ϵ) and the steady-state vaccinated population (V_h^*). The relationship is characterized by a strongly concave, non-linear decay. This inverse relationship is mechanistically driven by the role of ϵ in the force of infection (λ_h). An increase in ϵ raises the risk of infectious bites for all individuals, including those who are vaccinated. While the vaccine offers partial protection (modulated by efficacy σ_h), a sufficiently high contact rate overwhelms this protection, leading to a sharp increase in breakthrough infections. This effect manifests in the model as a critical outflow pathway from the V_h compartment: vaccinated individuals experience breakthrough infections and transition to the exposed (E_h) class. Consequently, the steady-state balance shifts; the constant inflow into V_h (from vaccination) is counteracted by an accelerated outflow due to infection, in addition to the baseline outflows from waning immunity (ξ_h) and mortality (μ_h). The precipitous decline in V_h^* at low-to-mid values of ϵ demonstrates the vulnerability of vaccination programs in high-transmission settings. This analysis underscores that environmental transmission intensity is a primary constraint on vaccine-derived population immunity. Vaccination cannot be viewed as a standalone intervention. Its success is contingent upon effective integrated vector management to suppress the contact rate (ϵ) and maintain the protective benefit of vaccination. The results argue strongly for combining vaccination with aggressive vector control efforts to reduce the risk of breakthrough infections and ensure the long-term stability of the vaccinated cohort.

Figure 5.1d demonstrates a definitive inverse relationship between the vaccine-induced immunity waning rate (ξ_h) and the steady-state size of the vaccinated population (V_h^*), characterized by an exceptionally strong negative correlation ($r \approx -0.928$). The response is markedly non-linear, exhibiting a concave, decaying trend. The analysis reveals that the stability of the vaccinated cohort is acutely sensitive to the duration of immunity. Incremental increases in the waning rate, particularly at lower values, precipitate a disproportionately large decline in V_h^*. This sensitivity arises because ξ_h constitutes a direct outflow pathway from the V_h compartment; a higher waning rate accelerates the transition of vaccinated individuals back to the susceptible state (S_h), where they are once again at risk of infection. This establishes that the long-term effectiveness of a vaccination program is not solely dependent on the initial efficacy (σ_h) or uptake rate (ν_h), but is fundamentally constrained by the durability of the immune response it elicits. Consequently, developing vaccines that confer long-lasting immunity is paramount for achieving and sustaining high levels of population coverage and underscores the critical role of vaccine durability in public health strategy.

5.4. Non-autonomous System

In this section, MATLAB is used to solve the sixteen-dimensional optimality problem using an iterative forward-backward sweep method (FBSM) in conjunction with the fourth-order Runge-Kutta algorithm. The state system 4.2, the adjoint system 4.11, and the control equations 4.16 specified across the time interval $[0, 400]$ days make up this system, which represents a two-point BVP. Our objective is to identify the best control measures required to slow the population's spread of malaria outbreak.

Starting with initial conditions and an initial control guess, the equations of the non-autonomous system 4.2 are solved forward in time, because the optimality system has several time orientations. The adjoint system's equations, on the other hand, with terminal conditions 4.12, are calculated backward.

The weight constants κ_i and ψ_i, where $i = 1, 2$ and 3 of the objective functional are taken as follows: $\kappa_1 = 0.5, \kappa_2 = 0.25, \kappa_3 = 0.5, \psi_1 = 1000, \psi_2 = 500$ and $\psi_3 = 1000$ together with the parameter values in Table 3.1. These theoretical weights are used to simulate OCP. For a strong surveillance effect, we take $\theta_1 = 0.6$ day^{-1} and $\theta_2 = 0.4$ day^{-1}.

In this study, three distinct strategies are examined for the optimization of the objective functional 4.1. Each strategy incorporates the application of at least two optimal control measures. The strategies are:

- **Strategy A:** A combination of Insecticide-Treated Nets and Improved Diagnostic Surveillance (i.e. $\psi_1(t)$ and $\psi_2(t)$, with $\psi_3(t) = 0$).
- **Strategy B:** A combination of Insecticide-Treated Nets and Environmental Sanitation (i.e. $\psi_1(t)$ and $\psi_3(t)$, with $\psi_2(t) = 0$).
- **Strategy C:** A combination of Insecticide-Treated Nets, Improved Diagnostic Surveillance and Environmental Sanitation (i.e. $\psi_1(t),\ \psi_2(t)$ and $\psi_3(t)$).

According to World Health Organization, one essential and vital method for preventing and controlling malaria is the use of ITNs, $\psi_1(t)$. It serves as a personal protection measure against mosquito bites. Thus, this intervention decreases the effective contact between humans and mosquitoes release [80]. Hence, this control measure in included in each of the strategies.

5.4.1. Strategy A: A combination of Insecticide-Treated Nets and Improved Diagnostic Surveillance (i.e. $\psi_1(t)$ and $\psi_2(t)$, with $\psi_3(t) = 0$) .

Figure 5.2a illustrates the temporal progression of the asymptomatic infected humans (A_h) under Strategy A. The dashed red curve represents the baseline dynamics, where A_h rises sharply to a pronounced peak before settling into a persistently elevated endemic equilibrium. This outcome underscores the role of asymptomatic carriers in sustaining malaria transmission, as they form a substantial, largely undetected reservoir of infection. By contrast, the solid blue curve reflects the effects of the interventions of Strategy A. Here, the intervention markedly reduces the peak of asymptomatic infections and lowers the long-term equilibrium to a substantially diminished level. This indicates that Strategy A does not only curtails the hidden reservoir of infection but also weakens the overall force of transmission across the population.

Figure 5.2b illustrates the dynamics of the symptomatic, infectious human hosts (I_h) over a 400-day period. The plot shows two distinct trajectories: one representing the baseline scenario (dashed red line) and another representing the system under a specific control strategy (solid blue line). In the absence of control, population of symptomatic humans surges rapidly to a high peak, indicating a substantial clinical burden. This is followed by a pronounced decline as individuals recover or are treated, eventually stabilizing at a lower, yet persistent, endemic level. The implementation of the control strategy substantially mitigates the initial outbreak and maintains the infectious population at a consistently reduced level, highlighting the effectiveness of the intervention in reducing both the peak incidence and the long-term burden of symptomatic disease.

Figure 5.2c illustrates the trajectory of the treated human hosts (T_h) over a 400-day period. The plot compares the baseline scenario (dashed red line) with the system under control strategy A (solid blue line). In the absence of control, the treated population rises sharply and reaches a very high peak, indicating a substantial and immediate burden on the healthcare system as it responds to the outbreak. The subsequent decline is gradual, stabilizing at a high endemic level, which suggests a persistent, long-term demand for treatment resources. The implementation of the control strategy results in a dramatically reduced and delayed peak. More importantly, the strategy maintains the treated population at a consistently low level throughout the simulation, effectively mitigating the clinical burden and demonstrating the intervention's success in reducing the number of cases severe enough to require treatment.

Figure 5.2d illustrates the dynamics of the recovered human hosts (R_h) over a 400-day period. The plot compares the baseline scenario (dashed red line) with the system under control strategy A (solid blue line). In the absence of control, the recovered population exhibits a rapid and substantial increase, reaching a very high equilibrium. This growth is driven by the steady inflow of individuals from the infectious and treatment compartments (A_h, I_h, T_h) as they clear the infection. The implementation of the control strategy results in a significantly lower and slower accumulation of recovered individuals. This outcome is a direct consequence of the successful intervention, which reduces the number of new infections and people who can eventually recover. While this leads to a smaller recovered population, it reflects a substantially reduced overall disease burden, as transmission is effectively curtailed at the source, preventing individuals from entering the infectious stages in the first place.

The prevalence increases sharply and stabilizes at a high endemic equilibrium, reflecting an uncontrolled outbreak in the absence of interventions. By contrast, the implementation of the control interventions under Strategy A produces a substantial reduction in prevalence relative to the baseline. The epidemic curve peaks at a much lower level and remains consistently reduced throughout the simulation, thereby demonstrating the effectiveness of the strategy in alleviating the disease burden (see Figure5.2e).

Figure 5.2f shows the behavior of the infected mosquito population (I_m) over time under Strategy A. The dashed red curve represents the baseline scenario without interventions while the solid blue curve represents the outcome under Strategy A. The introduction of Strategy A results in a significant decline in the population of infected mosquito. This demonstrates the effectiveness of the control strategy in reducing the population of infected mosquitoes.

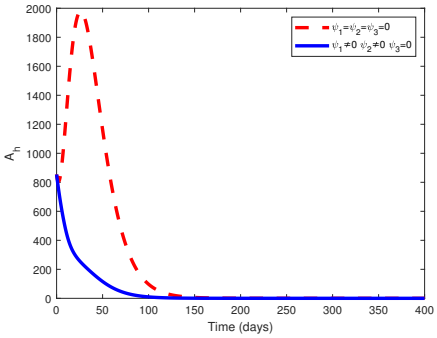

(a) Asymptomatic Humans

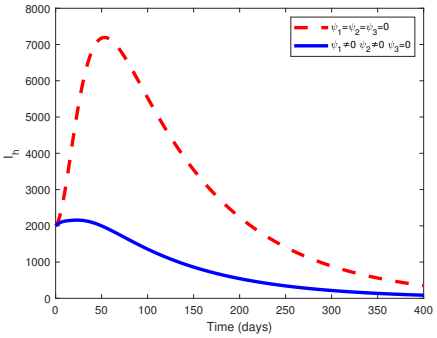

(b) Infected Humans

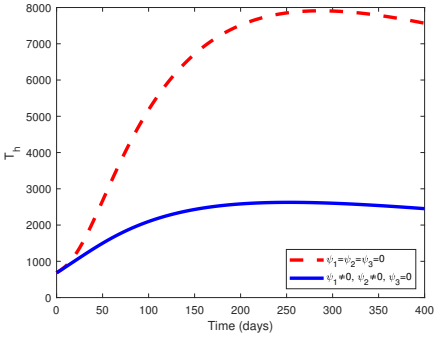

(c) Treated Humans

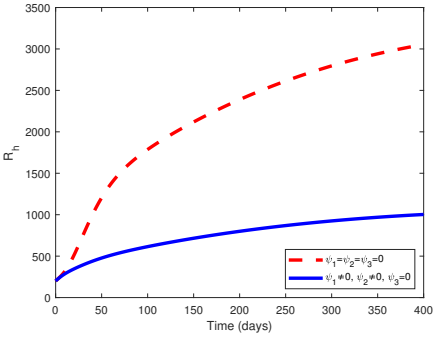

(d) Recovered Humans

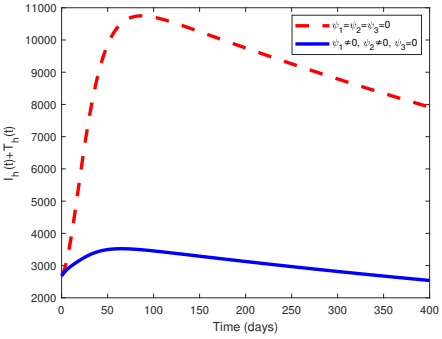

(e) Human Disease Prevalence

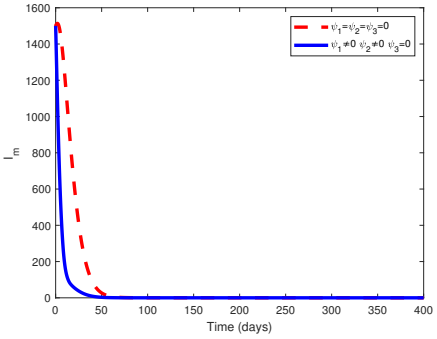

(f) Infected Mosquitoes

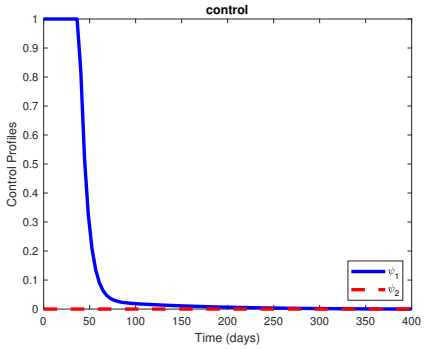

(g) Control Profiles

Figure 5.2. Effects of Strategy A on the Dynamics of Malaria Prevalence

The solid blue curve represents the control function, $\psi_1(t)$. It shows that this control is initially applied at the maximum possible intensity (a value of 1, indicating 100% effort or coverage) within the first 50 days. Thereafter, it declines to zero and remains at that level throughout the rest of the simulation. The dashed red curve represents the control function $\psi_2(t)$. This control is not activated at all for the entire duration, as its value remains at zero. This profile indicates that the optimal implementation of Strategy A requires the immediate and sustained application of control $\psi_1(t)$ at its highest possible level, while control $\psi_2(t)$ is determined to be unnecessary for this particular strategy and is therefore kept inactive (see Figure 5.2g).

5.4.2. Strategy B: A combination of Insecticide-Treated Nets and Environmental Sanitation (i.e. $\psi_1(t)$ and $\psi_3(t)$, with $\psi_2(t) = 0$). Figure 5.3a shows the dynamics of asymptomatic infections (A_h). Without intervention (dashed red), A_h peaks sharply and stabilizes at a high endemic level, sustained by a hidden reservoir of carriers. Under Strategy B (solid blue), both the peak and equilibrium are markedly reduced, demonstrating the intervention's effectiveness in shrinking this reservoir and weakening transmission.

Figure 5.3b presents the symptomatic infectious population (I_h). In the baseline, cases rise rapidly to a high peak and persist at an endemic level. Strategy B substantially lowers the peak and maintains a consistently reduced infectious population, alleviating both outbreak intensity and long-term burden.

Figure 5.3c illustrates treated cases (T_h). The baseline shows a sharp surge to a high peak, followed by a sustained demand on healthcare. With Strategy B, the peak is delayed and greatly diminished, and equilibrium levels remain low, reducing pressure on treatment resources.

Figure 5.3d depicts recovered individuals (R_h). The baseline results in a very high equilibrium due to continuous inflow from infections. Strategy B lowers recovery levels by preventing many infections from occurring, reflecting an overall reduction in the disease burden.

Figure 5.3e highlights overall prevalence. The baseline stabilizes at a high endemic level, while Strategy B keeps prevalence consistently suppressed, reducing both the epidemic peak and the equilibrium.

Figure 5.3f shows infected mosquitoes population (I_m). In the absence of these interventions, infections rise and persist at high levels. Strategy B reduces both the peak and equilibrium, demonstrating how human-focused measures also disrupt mosquito infection dynamics.

Figure 5.3g presents the optimal control profiles. It shows that the two controls, $\psi_1(t)$ and $\psi_2(t)$ are implemented immediately at full strength and maintained for approximately 50 days. Thereafter, they decline to zero and remain at that level for the rest of the simulation period. This pattern underscores the importance of sustained primary measures.

5.4.3. Strategy C: A combination of Insecticide-Treated Nets, Improved Diagnostic Surveillance and Environmental Sanitation (i.e. $\psi_1(t)$, $\psi_2(t)$ and $\psi_3(t)$). Figure 5.4a shows the dynamics of asymptomatic infections (A_h). Under the baseline (dashed red), A_h rises to a sharp peak and stabilizes at a high endemic equilibrium. With Strategy C (solid blue), the peak is strongly suppressed and the equilibrium driven close to zero. This indicates that combining ITNs, surveillance, and sanitation disrupts the hidden reservoir of infections and substantially weakens community transmission.

Figure 5.4b illustrates the symptomatic infectious population (I_h). Without intervention, symptomatic cases surge rapidly and persist at a significant endemic level. Strategy C does not only flattens the peak but also drives long-term symptomatic infections to very low levels, reflecting effective case detection and reduced exposure through vector control.

Figure 5.4c presents the treated population (T_h). In the baseline, treatment demand spikes sharply and stabilizes at a high level, indicating persistent strain on healthcare. Under Strategy C, the peak is dramatically reduced and the equilibrium remains minimal, demonstrating how combined measures ease clinical pressure by preventing both infection and progression.

Figure 5.4d depicts recovered individuals (R_h). The baseline shows a large recovered population, driven by high infection rates. Strategy C produces a much smaller recovery curve, reflecting the success of interventions in preventing infections upstream, rather than relying on recovery downstream.

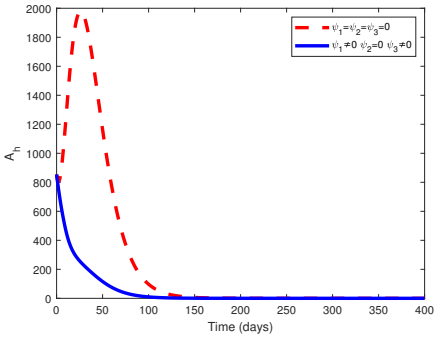

(a) Asymptomatic Humans

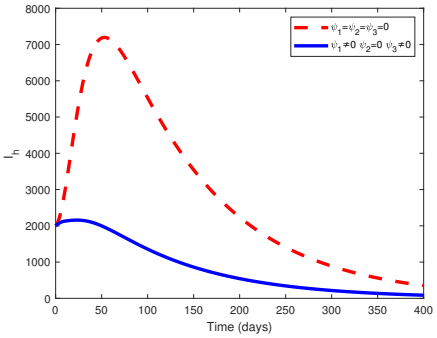

(b) Infected Humans

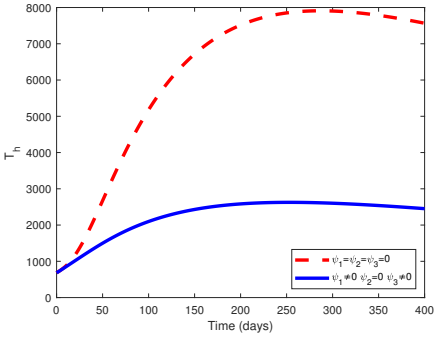

(c) Treated Humans

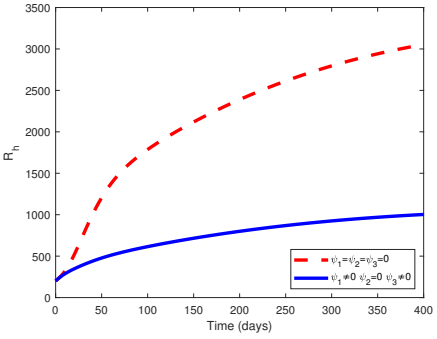

(d) Recovered Humans

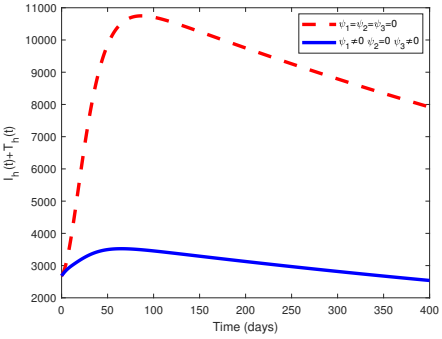

(e) Human Disease Prevalence

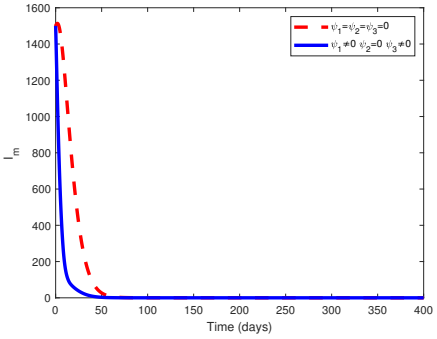

(f) Infected Mosquitoes

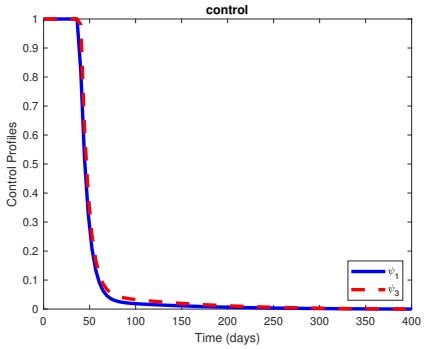

(g) Control Profiles

Figure 5.3. Effects of Strategy B on the Dynamics of Malaria Prevalence

]

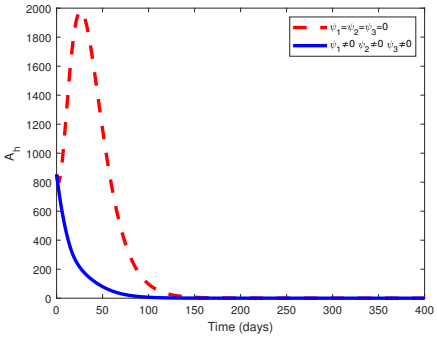

(a) Asymptomatic Humans

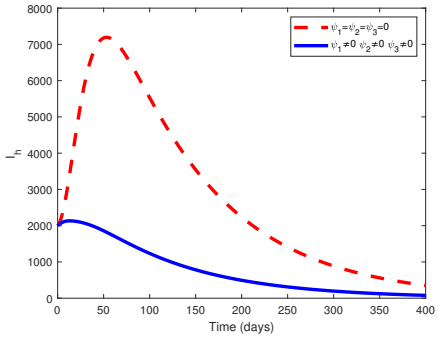

(b) Infected Humans

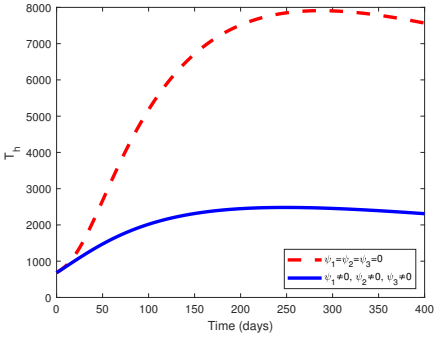

(c) Treated Humans

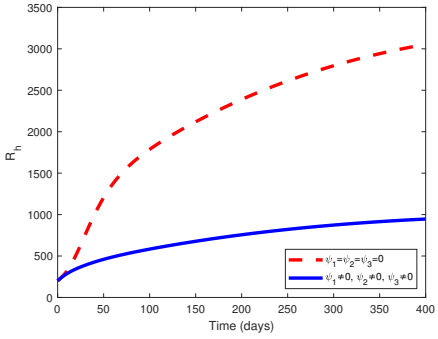

(d) Recovered Humans

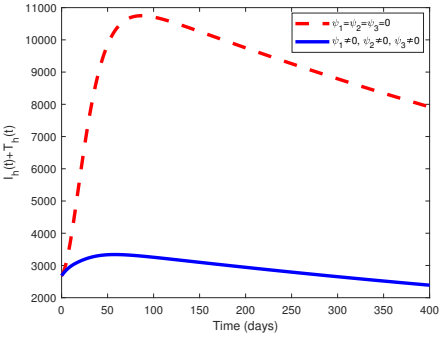

(e) Human Disease Prevalence

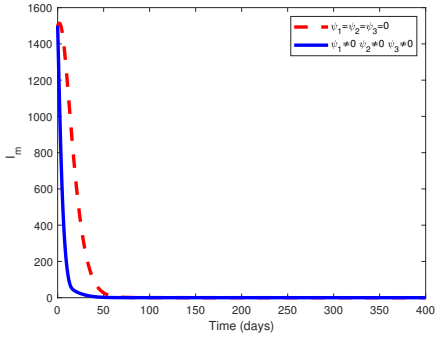

(f) Infected Mosquitoes

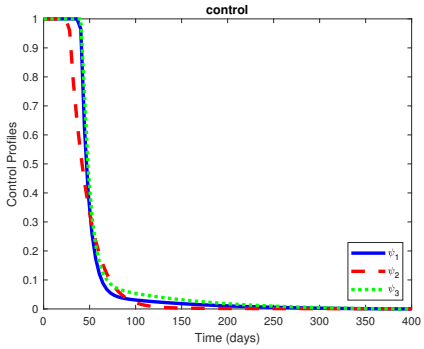

(g) Control Profiles

Figure 5.4. Effects of Strategy B on the Dynamics of Malaria Prevalence

Figure 5.4e highlights overall prevalence. In the baseline, prevalence climbs to a high endemic equilibrium. With Strategy C, both the epidemic peak and equilibrium are substantially lowered, keeping prevalence consistently near elimination levels throughout the simulation.

Figure 5.4f shows infected mosquitoes (I_m). Without intervention, mosquito infections persist at a high endemic level. Strategy C leads to a steep decline, with infections in the vector population driven close to zero, underscoring the impact of ITNs and environmental sanitation on breaking the mosquito−human transmission cycle.

Figure 5.4g presents the optimal control profiles. The controls, $\psi_1(t)$, $\psi_2(t)$, and $\psi_3(t)$, are applied immediately at full strength and sustained for a period before gradually declining to zero. This behavior emphasizes the importance of sustained control efforts at the early stage, followed by a tapering phase that maintains effectiveness while reducing intensity.

5.5. Cost-Effectiveness Analysis

The financial feasibility of several health interventions, such as ITNs, enhanced diagnostic surveillance, and environmental sanitation, was then assessed through a cost-effectiveness analysis. This type of research aids in determining whether the costs incurred are justified by the health advantages attained. Three key measures are evaluated in this section: the Infection Averted Ratio (IAR), the Average Cost-Effectiveness Ratio (ACER), and the Incremental Cost-Effectiveness Ratio (ICER) [9].

5.5.1. Infection Averted Ratio (IAR)

$$\text{IAR} = \frac{\text{Cumulative Cases Averted}}{\text{Total Number of Recovered Humans}} \tag{5.1}$$

The Cumulative Cases Averted is calculated by subtracting the total number of infectious individuals under the control strategy from those without any control. According to this analytical approach, the plan that offers the best cost-effectiveness has the highest IAR [9]. The IAR for each of the strategies is obtained by using the parameter values in Table 3.1.

Table 5.1 and Figure 5.6 present the results of the simulation. The highest IAR is obtained using Strategy B. Thus, the most cost-effective approach is strategy B according to this cost analysis technique. The next cost-effective strategy is C while the least economical approach is provided by Strategy A. Since Strategy A gives the smallest number of infection averted in the population, it is the least cost-effective, as shown in Table 5.1 and Figure 5.5.

Table 5.1. Strategy, Cumulative Cases Averted, Total Cost, IAR and ACER

Strategy	Cumulative Cases Averted	Total Cost ($)	IAR	ACER
$A : \psi_1(t), \psi_2(t)$	7335.34	100798.7701	0.0274	13.7415
$B : \psi_1(t), \psi_3(t)$	819609.27	547176.6786	2.8446	0.6676
$C : \psi_1(t), \psi_2(t), \psi_3(t)$	842285.47	171853.6889	2.6480	0.2040

5.5.2. Average Cost-Effectiveness Ratio (ACER) The cost necessary to stop one infection case with a particular intervention is represented by the ACER. It is calculated by dividing the total cost of putting a strategy into practice by the total number of infections that the approach effectively prevents.

$$\text{ACER} = \frac{\text{Total cost of implementing the strategy}}{\text{Total number of infections it successfully prevents}} \tag{5.2}$$

Given the objective functional in 4.1, the total cost generated by a strategy is stated as

$$\text{TC} = \int_0^{t_f} (\kappa_1\psi_1 N_h + \kappa_2\psi_2 E_h + \kappa_3\psi_3 N_m + \omega_1\psi_1^2 + \omega_2\psi_2^2 + \omega_3\psi_3^2)dt \tag{5.3}$$

A more effective and financially advantageous intervention is indicated by a lower ACER value [9]. The ACER for each of the three interventions is thus determined using equation 5.2. The numerical results of the simulation are shown in Table 5.1 and Figure 5.8.

According to this cost analysis method, Strategy C is the most cost-effective approach because it has the lowest ACER. Strategy B comes next. Stragegy A is the least cost-effective strategy because it has the highest ACER.

The following method is used to confirm these findings through additional cost-effectiveness analysis.

Table 5.2. Strategy, Cumulative Cases Averted, Total Cost and ICER

Strategy	Cumulative Cases Averted	Total Cost ($)	ICER
$A : \psi_1(t), \psi_2(t)$	7335.34	100798.7701	13.7415
$B : \psi_1(t), \psi_3(t)$	819609.27	547176.6786	0.5495
$C : \psi_1(t), \psi_2(t), \psi_3(t)$	842285.47	171853.6889	-16.5560

5.5.3. Incremental Cost-Effectiveness Ratio (ICER) A new health intervention's cost-effectiveness is evaluated using the ICER in comparison to a baseline or conventional method. It is described as

$$\text{ICER} = \frac{\text{Total cost with control-Total cost without control}}{\text{Total number of infections without control-Total number of infections with control}} \tag{5.4}$$

We calculate the ICER for each strategy using the formula provided by equation 5.4 and the methods in [9].

$$\text{ICER(A)} = \frac{100798.7701}{7335.34} = 13.7415$$

$$\text{ICER(B)} = \frac{547176.6786 - 100798.7701}{819609.27 - 7335.34} = \frac{446377.9085}{812273.93} = 0.5495$$

$$\text{ICER(C)} = \frac{171853.6889 - 547176.6786}{842285.47 - 819609.27} = -16.5560$$

Table 5.2 compares Strategies A and B and reveals that ICER(A) is higher than ICER(B). This indicates that Strategy B is in control of Strategy A. As a result, Strategy B is more cost-effective. Hence, Strategy A is excluded in further analysis.

Thus, we are left with Strategies B and C. Using equation 5.4, Table 5.3 provides the ICER summary for the two Strategies. From Table 5.3, is can be seen that Strategy C's ICER is lower than Strategy B's. This implies that Strategy C is more economical than Strategy B, Strategy B is thus eliminated from the list. Therefore, Strategy C is the most economical.

Strategy C, which combines the best use of insecticide-treated nets, improved diagnostic surveillance, and environmental sanitation (i.e., $\psi_1(t)$, $\psi_2(t)$, and $\psi_3(t)$) is the most cost-effective strategy since it produced the least ICER.

Table 5.3. Performance Comparison of Strategies B and C

Strategy	Cumulative Cases Averted	Total Cost ($)	ICER
$B : \psi_1(t), \psi_3(t)$	819609.27	547176.6786	0.6676
$C : \psi_1(t), \psi_2(t), \psi_3(t)$	842285.47	171853.6889	16.5560

6. Conclusion

This study developed and analyzed a nonlinear mathematical model for malaria transmission dynamics that incorporates a vaccinated human class alongside conventional interventions. The autonomous system was shown

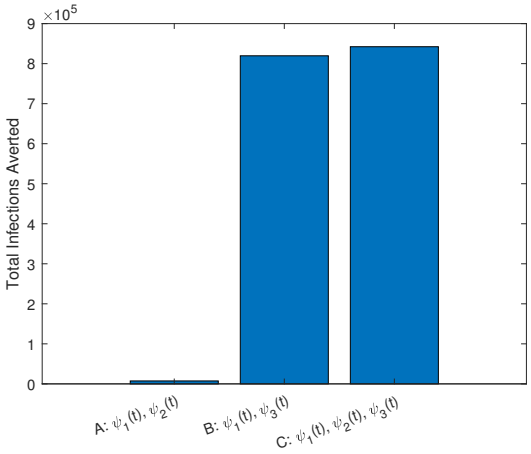

Figure 5.5. Plots of Cumulative Cases Averted for Strategies A, B and C

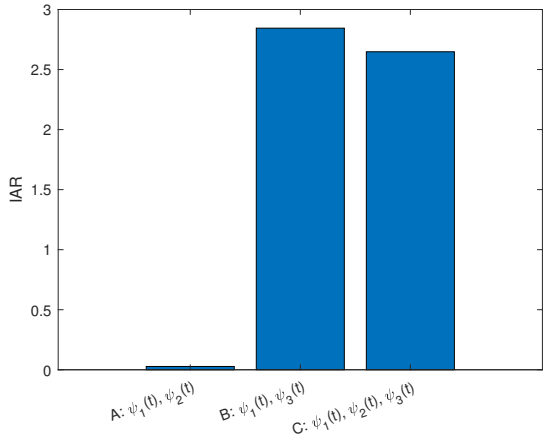

Figure 5.6. Plots of IAR for Strategies A, B and C

to be mathematically well-posed: all solutions remain positive and bounded in a biologically feasible region. Using the Next-Generation Matrix method, the effective reproduction number R_e was derived and it was established that the DFE is locally and GAS whenever $R_e < 1$. Conversely, a unique endemic equilibrium exists and is globally stable when $R_e > 1$. These results confirm that malaria elimination or persistence is determined by the threshold value of R_e in the autonomous system.

The sensitivity analysis identified the most influential parameters on the disease spread, including vaccine uptake ν_h, efficacy σ_h, waning immunity ξ_h and mosquito$-$human contact rate ϵ. Numerical simulations demonstrated that vaccination reduces the burden of malaria infection and sustains lower transmission levels over time, with greater benefits achieved as uptake and efficacy increase.

The model was further extended to a non-autonomous system through the incorporation of three time-dependent control strategies. Optimal-control analysis revealed that while single or dual interventions yield moderate reductions in prevalence, the integrated triple strategy (vaccination, vector control, and treatment/environmental measures) provides the greatest epidemiological impact. Cost-effectiveness analysis using IAR, ACER and ICER showed that this integrated non-autonomous strategy is not only the most effective but also the most economically efficient.

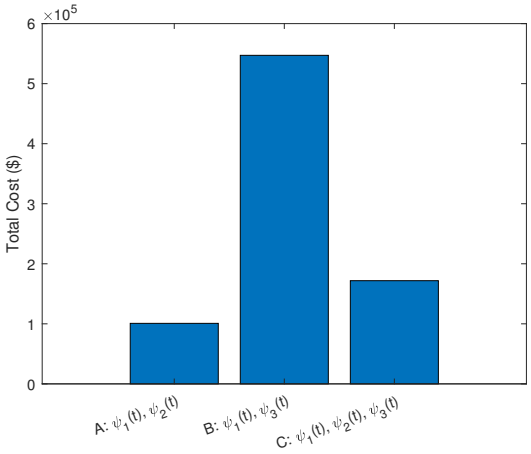

Figure 5.7. Plots of Total Cost for Strategies A, B and C

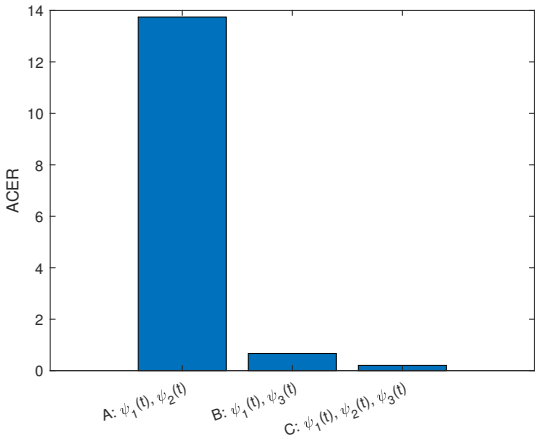

Figure 5.8. Plots of ACER for Strategies A, B and C

The autonomous analysis highlights the threshold conditions governing malaria persistence, while the non-autonomous optimal-control framework demonstrates how integrated, time-dependent interventions can drive malaria elimination in a cost-effective manner. Policymakers and healthcare practitioners are encouraged to adopt combined strategies that strengthen vaccination coverage and durability while sustaining vector management and treatment efforts to achieve long-term malaria control and eventual eradication.

REFERENCES

1. Peter Aaby, Ane B Fisker, Anders Björkman, and Christine Stabell Benn. Who's rollout of malaria vaccine in africa: can safety questions be answered after only 24 months? *BMJ*, 368, 2020.
2. Mohammed Baba Abdullahi, Yahya Abu Hasan, and Farah Aini Abdullah. A mathematical model of malaria. *Applied Mathematical Sciences*, 7(62):3079–3095, 2013.
3. M. M. Abdulrahman et al. Malaria infection rate in mosquitoes in relation to transmission in gombe south, gombe state, nigeria. *Dutse Journal of Pure and Applied Sciences*, 10(1):52–61, 2024. Accessed: 2025-08-13.
4. A Abidemi, JO Akanni, and OD Makinde. A non-linear mathematical model for analysing the impact of covid-19 disease on higher education in developing countries. *Healthcare Analytics*, 3:100193, 2023.

5. Gbenga Adegbite, Sunday Edeki, Itunuoluwa Isewon, Jerry Emmanuel, Titilope Dokunmu, Solomon Rotimi, Jelili Oyelade, and Ezekiel Adebiyi. Mathematical modeling of malaria transmission dynamics in humans with mobility and control states. *Infectious Disease Modelling*, 8(4):1015–1031, 2023.
6. A. Adikari and Y. Jayathunga. Optimal control for resource allocation in a multi-patch epidemic model with human dispersal behavior. *Communication in Biomathematical Sciences*, 8(1):1–18, 2025.
7. Agnes Adom-Konadu, Ernest Yankson, Samuel M Naandam, and Duah Dwomoh. A mathematical model for effective control and possible eradication of malaria. *Journal of Mathematics*, 2022(1):6165581, 2022.
8. Pardi Affandi et al. Optimal control mathemathical sir model of malaria spread in south kalimantan. In *Journal of physics: conference series*, volume 1116, page 022001. IOP Publishing, 2018.
9. Ayodeji Sunday Afolabi and Miswanto Miswanto. Mathematical modeling, optimal control and cost-effectiveness analysis of diphtheria transmission dynamics. *Jambura Journal of Biomathematics (JJBM)*, 6(2):88–108, 2025.
10. Mary Oluwabunmi Akinade and Ayodeji Sunday Afolabi. Sensitivity and stability analyses of a lassa fever disease model with control strategies. *IOSR Journal of Mathematics (IOSR-JM)*, 16(1):29–42, 2020.
11. Mary Oluwabunmi Akinade, Ayodeji Sunday Afolabi, and Mark Eric Kimathi. Mathematical modeling and stability analyses of lassa fever disease with the introduction of the carrier compartment. *Mathematical Theory and Modeling*, 9(6):45–62, 2019.
12. Folake O Akinpelu and Richard Akinwande. Mathematical model for lassa fever and sensitivity analysis. *J. Sci. Eng. Res*, 5(6):1–9, 2018.
13. Maha A Al-Moneef and Salihah A Al-Sheikh. Mathematical modeling of malaria transmission with age-structured human population. *Computational and Mathematical Methods in Medicine*, 2023, 2023.
14. Hussam Alrabaiah, Mohammad A Safi, Mahmoud H DarAssi, Bashir Al-Hdaibat, Saif Ullah, Muhammad Altaf Khan, and Syed Azhar Ali Shah. Optimal control analysis of hepatitis b virus with treatment and vaccination. *Results in Physics*, 19:103599, 2020.
15. Alex Altamirano-Fernández, Alejandro Rojas-Palma, and Sergio Espinoza-Meza. Existence of solutions for an optimal control problem in forestry management. In *Journal of Physics: Conference Series*, volume 2515, page 012001, Bristol, UK, 2023. IOP Publishing.
16. T. S. Awolola et al. Vector competence of anopheles gambiae s.l. in lagos, nigeria. *Journal of Vector Borne Diseases*, 43(2):91–94, 2006.
17. Muhamad Adzib Baihaqi and Fajar Adi-Kusumo. Modelling malaria transmission in a population with seirsp method. In *AIP conference proceedings*, volume 2264. AIP Publishing, 2020.
18. EA Bakare and CR Nwozo. Bifurcation and sensitivity analysis of malaria–schistosomiasis co-infection model. *International Journal of Applied and Computational Mathematics*, 3:971–1000, 2017.
19. Olufemi F. Bamiselu, Isaac O. Ajayi, Olufunmilayo Fawole, David M. Dairo, O. Oladimeji, Omotayo Ajumobi, Akin Oyemakinde, C. Umeh, P. Onyiah, and Adebola Olayinka. Adherence to malaria diagnosis and treatment guidelines among healthcare workers in ogun state, nigeria. *Malaria Journal*, 16(394):1–10, 2017.
20. BE Bassey, JE Asor, and MF Useh. Profile of malaria in pregnant women attending antenatal clinics in rural community in nigeria. *The Open Parasitology Journal*, 1(1), 2007.
21. Maciej F Boni, Caroline O Buckee, and Nicholas J White. Mathematical models for a new era of malaria eradication. *PLoS Medicine*, 5(11):e231, 2008.
22. Daniel Chandramohan, Issa Zongo, et al. Comparative efficacy of malaria vaccines rts,s/as01 and r21/matrix-m: evidence from trials in african children. *PLOS Medicine*, 21(1):e1004515, 2024. Accessed: 2025-09-01.
23. Nakul Chitnis, Allan Schpira, David Smith, Simon I Hay, Thomas Smith, Richard Steketee, et al. Mathematical modelling to support malaria control and elimination. 2010.
24. Rima Devi and Balendra Kumar Dev Choudhury. Analysis of sir mathematical model for malaria disease: A study in assam, india. *Jurnal ILMU DASAR*, 24(2):169–174, 2023.
25. Titilope M Dokunmu, Cynthia U Adjekukor, Omolara F Yakubu, Adetutu O Bello, Jarat O Adekoya, Olugbenga Akinola, Emmanuel O Amoo, and Abiodun H Adebayo. Asymptomatic malaria infections and pfmdr1 mutations in an endemic area of nigeria. *Malaria journal*, 18(1):218, 2019.
26. Pride Duve, Samuel Charles, Justin Munyakazi, Renke Lühken, and Peter Witbooi. A mathematical model for malaria disease dynamics with vaccination and infected immigrants. *Mathematical Biosciences and Engineering*, 21(1):1082–1109, 2024.
27. Jacob O. Fadare, Olakunle Olatunde, Adebowale Adeoti, Funmilayo Adeoti, Dahiru Garba, and Adebola E. Orimadegun. Facility-based malaria case management practices in nigeria. *Malaria Journal*, 22(295):1–10, 2023.
28. Wendell H Fleming and Raymond W Rishel. *Deterministic and Stochastic Optimal Control*, volume 1. Springer Science & Business Media, New York, USA, 2012.
29. D. Garba et al. Vector competence and sporozoite rates of anopheles mosquitoes in north-west nigeria. *Parasitology International*, 92:102731, 2023.
30. Abba B Gumel and Suzanne Lenhart. *Modeling Paradigms and Analysis of Disease Transmission Models*, volume 75. American Mathematical Society, Providence, USA, 2010.
31. Jericho Hallare and Valerie Gerriets. Half life. *StatPearls*, 2020. Accessed April 29, 2025.
32. HealthKnowledge Public Health Textbook. Epidemiology of infectious diseases: Malaria. https://www.healthknowledge.org.uk/index.php/public-health-textbook/disease-causation-diagnostic/2b-epidemiology-diseases-phs/infectious-diseases/malaria, 2025. Accessed: 2025-08-15.
33. Malik Muhammad Ibrahim, Muhammad Ahmad Kamran, Malik Muhammad Naeem Mannan, Sangil Kim, and Il Hyo Jung. Impact of awareness to control malaria disease: A mathematical modeling approach. *Complexity*, 2020(1):8657410, 2020.
34. Athassawat Kammanee and Orawan Tansuiy. A mathematical model of transmission of plasmodium vivax malaria with a constant time delay from infection to infectious. *Communications of the Korean Mathematical Society*, 34(2):685–699, 2019.
35. Ebrima Kanyi, Ayodeji Sunday Afolabi, and Nelson Owuor Onyango. Optimal control analysis of schistosomiasis dynamics. *J. Math. Comput. Sci.*, 11(4):4599–4630, 2021.

36. George A Korsah and Bright K Lawson. Mathematical modeling of malaria transmission with asymptomatic carriers and temperature-dependent parameters. *Infectious Disease Modelling*, 9(1):1–18, 2024.
37. Suzanne Lenhart and John T Workman. *Optimal control applied to biological models*. Chapman and Hall/CRC, Boca Raton, FL, USA, 2007.
38. Rhea J Longley, Josephine Malinga, Eva Hesping, Edwin Sutanto, Sophia M DonVito, Michal Kucharski, Damian A Oyong, Julie MJ Verhoef, Esrah Du, Elizabeth Villasis, et al. Mam 2024: Malaria in a changing world. *Trends in Parasitology*, 2024.
39. Yijun Lou and Xiao-Qiang Zhao. Modelling malaria control by introduction of larvivorous fish. *Bulletin of mathematical biology*, 73(10):2384–2407, 2011.
40. Sandip Mandal, Ram Rup Sarkar, and Somdatta Sinha. Mathematical models of malaria-a review. *Malaria journal*, 10:1–19, 2011.
41. Antônio Ralph Medeiros-Sousa, Gabriel Zorello Laporta, Renato Mendes Coutinho, Luis Filipe Mucci, and Mauro Toledo Marrelli. A mathematical model for zoonotic transmission of malaria in the atlantic forest: Exploring the effects of variations in vector abundance and acrodendrophily. *PLoS neglected tropical diseases*, 15(2):e0008736, 2021.
42. Cristhian Montoya and Jhoana P Romero-Leiton. Mathematical modelling for malaria under resistance and population movement. *Revista Integración*, 38(2):133–163, 2020.
43. Egide Ndamuzi and Paterne Gahungu. Mathematical modeling of malaria transmission dynamics: case of burundi. *Journal of applied mathematics and physics*, 9(10):2447–2460, 2021.
44. Meksianis Z Ndii and Samson Olaniyi. Using mathematical models to understand, assess, and mitigate vector-borne diseases, 2023.
45. Gideon A Ngwa and William S Shu. A mathematical model for endemic malaria with variable human and mosquito populations. *Mathematical and computer modelling*, 32(7-8):747–763, 2000.
46. NOI Polls. Malaria disease: A worrisome health challenge in nigeria. https://www.noi-polls.com/post/malaria-disease-a-worrisome-health-challenge-in-nigeria, 2022. Accessed: 2025-08-13.
47. K. Oduro, S. C. Noutchie, and A. Nwankwo. A malaria transmission model with mosquito mortality induced by insecticide-treated nets. *Journal of Applied Mathematics*, 2024:1–21, 2024.
48. Festus Abiodun Oguntolu, Olumuyiwa James Peter, Benjamin Idoko Omede, Ghaniyyat Bolanle Balogun, Aminat Olabisi Ajiboye, and Hasan S Panigoro. Mathematical modeling on the transmission dynamics of diphtheria with optimal control strategies. *Jambura Journal of Biomathematics (JJBM)*, 6(1):1–22, 2025.
49. Mayowa M Ojo and Emile Franc Doungmo Goufo. Assessing the impact of control interventions and awareness on malaria: a mathematical modeling approach. *Commun. Math. Biol. Neurosci.*, 2021:Article–ID, 2021.
50. R. O. Ojutiku et al. Malaria transmission dynamics and sporozoite rates in anyigba, kogi state, nigeria. *Journal of Parasitology Research*, 2016:Article ID 3245179, 2016.
51. Segun I Oke, Michael M Ojo, Michael O Adeniyi, and Maba B Matadi. Mathematical modeling of malaria disease with control strategy. *Commun. Math. Biol. Neurosci.*, 2020:Article–ID, 2020.
52. S Olaniyi and OS Obabiyi. Mathematical model for malaria transmission dynamics in human and mosquito populations with nonlinear forces of infection. *International journal of pure and applied Mathematics*, 88(1):125–156, 2013.
53. Idowu K Oluwatobi et al. Mathematical modelling of the transmission dynamics of malaria infection with optimal control. *Kathmandu University Journal of Science, Engineering and Technology*, 15(3), 2021.
54. Nkechi Onyedika-Ugoeze. Nigeria accounts for 31% of malaria deaths, 27% of total cases worldwide. *The Guardian Nigeria*, April 2025. Online.
55. World Health Organization. *Global technical strategy for malaria 2016-2030*. World Health Organization, 2015.
56. World Health Organization. *Report of the first and second meetings of the technical advisory group on malaria elimination and certification, 13–14 September 2022 and 27 January 2023*. World Health Organization, 2023.
57. World Health Organization. *Global Malaria Programme operational strategy 2024-2030*. World Health Organization, 2024.
58. World Health Organization et al. Who initiative to stop the spread of anopheles stephensi in africa. In *WHO initiative to stop the spread of Anopheles stephensi in Africa*. 2023.
59. World Health Organization et al. World malaria report 2024: addressing inequity in the global malaria response. 2024.
60. Josiah C. Orji, T.T. Yusuf, **Afolabi, A.S.**, and K.A. Dawodu. Integrated malaria control: impacts of vaccination and combined interventions on disease dynamics. *Modeling Earth Systems and Environment*, 11(6):1–23, 2025.
61. Mojeeb Osman and Isaac Adu. Simple mathematical model for malaria transmission. *Journal of Advances in Mathematics and Computer Science*, 25(6):1–24, 2017.
62. Caroline Bonareri Osoro, Eleanor Ochodo, Titus K Kwambai, Jenifer Akoth Otieno, Lisa Were, Caleb Kimutai Sagam, Eddy Johnson Owino, Simon Kariuki, Feiko O Ter Kuile, and Jenny Hill. Policy uptake and implementation of the rts, s/as01 malaria vaccine in sub-saharan african countries: status 2 years following the who recommendation. *BMJ Global Health*, 9(4):e014719, 2024.
63. Ifeoma D Ozodiegwu, Monique Ambrose, Beatriz Galatas, Manuela Runge, Aadrita Nandi, Kamaldeen Okuneye, Neena Parveen Dhanoa, Ibrahim Maikore, Perpetua Uhomoibhi, Caitlin Bever, et al. Application of mathematical modelling to inform national malaria intervention planning in nigeria. *Malaria journal*, 22(1):137, 2023.
64. Carla MA Pinto and JA Tenreiro Machado. Fractional model for malaria transmission under control strategies. *Computers & Mathematics with Applications*, 66(5):908–916, 2013.
65. Queensland Health. Malaria. https://www.health.qld.gov.au/cdcg/index/malaria, 2025. Accessed: 2025-08-15.
66. S Clinical Trials Partnership RTS. Efficacy and safety of rts,s/as01 malaria vaccine with or without a booster dose in infants and children in africa: final results of a phase 3, individually randomised, controlled trial. *PLOS Medicine*, 11(7):e1001685, 2014. Accessed: 2025-09-01.
67. A. Samuel et al. Sporozoite infection rates in anopheles mosquitoes in guinea and sudan savanna zones of adamawa state, nigeria. *Acta Tropica*, 218:105905, 2021.
68. Zadoki Tabo, Livingstone S Luboobi, and Joseph Ssebuliba. Mathematical modelling of the in-host dynamics of malaria and the effects of treatment. 2017.
69. Stephane Y Tchoumi, CW Chukwu, Mamadou L Diagne, Herieth Rwezaura, ML Juga, and Jean M Tchuenche. Optimal control of a two-group malaria transmission model with vaccination. *Network Modeling Analysis in Health Informatics and Bioinformatics*,

12(1):7, 2022.
70. Halidou Tinto, Umberto D'Alessandro, et al. Efficacy and safety of r21/matrix-m malaria vaccine in african children: a multicentre, double-blind, randomised, controlled, phase 3 trial. *The Lancet*, 403(10431):185–197, 2024. Accessed: 2025-09-01.
71. Bakary Traoré, Moussa Barro, Boureima Sangaré, and Sado Traoré. A temperature-dependent mathematical model of malaria transmission with stage-structured mosquito population dynamics. *Nonautonomous Dynamical Systems*, 8(1):267–296, 2021.
72. Bakary Traoré, Boureima Sangaré, and Sado Traoré. A mathematical model of malaria transmission with structured vector population and seasonality. *Journal of Applied Mathematics*, 2017(1):6754097, 2017.
73. Julius Tumwiine, JYT Mugisha, and Livingstone S Luboobi. A mathematical model for the dynamics of malaria in a human host and mosquito vector with temporary immunity. *Applied mathematics and computation*, 189(2):1953–1965, 2007.
74. United Nations Department of Economic and Social Affairs. *World Population Prospects 2023*. UN DESA, 2023.
75. Crankson Monica Veronica, Olotu Olusegun, Amegbey Newton, and Afolabi Ayodeji Sunday. Mathematical modeling and stability analyses on the transmission dynamics of bacterial meningitis. *J. Math. Comput. Sci.*, 11(6):7384–7413, 2021.
76. Wikipedia contributors. Plasmodium falciparum. https://en.wikipedia.org/wiki/Plasmodium_falciparum, 2025. Accessed: 2025-08-15.
77. World Bank. Life expectancy at birth - nigeria (2015-2022), 2024. Accessed July 2024.
78. World Health Organization. Nigeria malaria report 2023. 2023.
79. World Health Organization. R21/matrix-m malaria vaccine: Global advisory committee on vaccine safety (gacvs). https://www.who.int/groups/global-advisory-committee-on-vaccine-safety/topics/malaria-vaccines/r21-matrix-m-vaccine, 2023. Accessed: 2025-09-01.
80. World Health Organization. Who publishes recommendations on two new types of insecticide-treated nets. https://www.who.int/news/item/14-03-2023-who-publishes-recommendations-on-two-new-types-of-insecticide-treated-nets, 2023. Accessed: 2025-08-23.
81. World Health Organization. World health statistics: Nigeria (2015-2023), 2023.
82. Yanyu Xiao. *Study of malaria transmission dynamics by mathematical models*. The University of Western Ontario (Canada), 2011.
83. Zhenbu Zhang and Tor A Kwembe. Qualitative analysis of a mathematical model for malaria transmission and its variation. In *Tenth MSU Conference on Differential Equations and Computation Simulations. Electronic Journal of Differential Equations, Conference*, volume 23, pages 195–210, 2016.
84. Zhihong Zhao, Shaochun Li, and Yulan Lu. Mathematical models for the transmission of malaria with seasonality and ivermectin. 2022.